

 Open access • Posted Content • DOI:10.1101/2020.11.17.377705

## **USP28 deletion and small molecule inhibition destabilises c-Myc and elicits regression of squamous cell lung carcinoma — Source link**

E. Josue Ruiz, Adan Pinto-Fernandez, Andrew P. Turnbull, Linxiang Lan ...+27 more authors

**Institutions:** Francis Crick Institute, University of Oxford, Max Planck Society, Walter and Eliza Hall Institute of Medical Research ...+1 more institutions

**Published on:** 18 Nov 2020 - bioRxiv (Cold Spring Harbor Laboratory)

Related papers:

- [Ubiquitin-specific peptidase 46 \(USP46\) suppresses renal cell carcinoma tumorigenesis through AKT pathway inactivation.](#)
- [Deubiquitinase USP18 Loss Mislocalizes and Destabilizes KRAS in Lung Cancer.](#)
- [Ubiquitin specific peptidase 49 inhibits non-small cell lung cancer cell growth by suppressing PI3K/AKT signaling](#)
- [Ubiquitin-specific peptidase 17 promotes cisplatin resistance via PI3K/AKT activation in non-small cell lung cancer.](#)
- [Ubiquitin specific peptidase 5 promotes ovarian cancer cell proliferation through deubiquitinating HDAC2.](#)

Share this paper:    

View more about this paper here: <https://typeset.io/papers/usp28-deletion-and-small-molecule-inhibition-destabilises-c-4q9p5gayqn>

1 **USP28 deletion and small molecule inhibition destabilises c-Myc and elicits**  
2 **regression of squamous cell lung carcinoma**

3  
4 E. Josue Ruiz<sup>1</sup>, Adan Pinto-Fernandez<sup>2</sup>, Andrew P. Turnbull<sup>3</sup>, Linxiang Lan<sup>1</sup>, Thomas  
5 M. Charlton<sup>2</sup>, Hannah Claire Scott<sup>2</sup>, Andreas Damianou<sup>2</sup>, George Vere<sup>2</sup>, Eva M.  
6 Riising<sup>1</sup>, Clive Da Costa<sup>1</sup>, Wojciech W. Krajewski<sup>3</sup>, David Guerin<sup>4,12</sup>, Jeffrey Kearns<sup>4,13</sup>,  
7 Stephanos Ioannidis<sup>4,14</sup>, Marie Katz<sup>4,15</sup>, Crystal McKinnon<sup>4,15</sup>, Jonathan C.  
8 O'Connell<sup>4,15</sup>, Natalia Moncaut<sup>1</sup>, Ian Rosewell<sup>5</sup>, Emma Nye<sup>1</sup>, Neil Jones<sup>3</sup>, Claire  
9 Heride<sup>3</sup>, Malte Gersch<sup>6</sup>, Min Wu<sup>16</sup>, Christopher J. Dinsmore<sup>4,17</sup>, Tim R. Hammonds<sup>3,18</sup>,  
10 Sunkyu Kim<sup>19</sup>, David Komander<sup>7</sup>, Sylvie Urbé<sup>8</sup>, Michael J. Clague<sup>9</sup>, Benedikt M.  
11 Kessler<sup>2,20</sup> and Axel Behrens<sup>1,9,10,11,20</sup>  
12

13 <sup>1</sup> Adult stem cell laboratory; The Francis Crick Institute, 1 Midland Road, London NW1 1AT, UK

14 <sup>2</sup> Target Discovery Institute, Nuffield Department of Medicine, University of Oxford, Roosevelt  
15 Drive, Oxford OX3 7FZ, UK

16 <sup>3</sup> CRUK Therapeutic Discovery Laboratories, The Francis Crick Institute, 1 Midland Road, London  
17 NW1 1AT, UK

18 <sup>4</sup> FORMA Therapeutics, Arsenal Street, Watertown, Massachusetts 02472, USA

19 <sup>5</sup> Genetic Manipulation Service, The Francis Crick Institute, 1 Midland Road, London NW1 1AT,  
20 UK

21 <sup>6</sup> Max Planck Institute of Molecular Physiology, Otto-Hahn-Str 11, 44227 Dortmund, Germany

22 <sup>7</sup> Ubiquitin Signalling Division, Walter and Eliza Hall Institute of Medical Research, Royal Parade,  
23 Parkville VIC 3052, and Dept of Medical Biology, University of Melbourne, VIC 3010, Australia

24 <sup>8</sup> Cellular and Molecular Physiology, Institute of Translational Medicine, University of Liverpool,  
25 Crown Street, Liverpool L69 3BX, UK

26 <sup>9</sup> Cancer Stem Cell Laboratory, Institute of Cancer Research, London, UK

27 <sup>10</sup> Imperial College, Division of Cancer, Department of Surgery and Cancer, London, UK

28 <sup>11</sup> Convergence Science Centre, Imperial College, London, SW7 2BU, UK

29 <sup>12</sup> Present address: Constellation Pharmaceuticals, 215 First St, Cambridge, MA 02142, USA

30 <sup>13</sup> Present address: Novartis Institutes for BioMedical Research, 250 Massachusetts Ave,  
31 Cambridge, MA 02139, USA

32 <sup>14</sup> Present address: H3 Biomedicine, 300 Technology Square, Cambridge, MA 02139, USA

33 <sup>15</sup> Present address: Valo Health, 399 Boylston St, Suite 505, Boston, MA 02116, USA

34 <sup>16</sup> Present address: Disc Medicine, 150 Cambridgepark Drive Suite 103, Cambridge, MA 02135,  
35 USA

36 <sup>17</sup> Present address: Kronos Bio, Inc., 301 Binney Street, 2nd Floor East, Cambridge, MA 02142,  
37 USA

38 <sup>18</sup> Present address: Locki Therapeutics, London Bioscience Innovation Centre, 2 Royal College  
39 Street, London NW1 0NH, UK

40 <sup>19</sup>Incyte, 1801 Augustine Cut-off, Wilmington, DE 19803, USA

41 <sup>20</sup>:

42	Benedikt M Kessler	Axel Behrens
43	Target Discovery Institute	The Francis Crick Institute
44	University of Oxford	London
45	OX3 7FZ, UK	NW1 AT, UK
46	<a href="mailto:benedikt.kessler@ndm.ox.ac.uk">benedikt.kessler@ndm.ox.ac.uk</a>	<a href="mailto:axel.behrens@icr.ac.uk">axel.behrens@icr.ac.uk</a>

47

48

49 **Running title:** Essential function of USP28 in squamous cell lung cancer

1 **Abstract** (188 words)

2 Lung squamous cell carcinoma (LSCC) is a considerable global health burden, with  
3 an incidence of over 600,000 cases per year. Treatment options are limited, and  
4 patient 5-year survival rate is less than 5%. The ubiquitin specific protease 28 (USP28)  
5 has been implicated in tumorigenesis through its stabilization of the oncoprotein c-  
6 MYC. Here, we show that genetic inactivation of *Usp28* induced regression of  
7 established murine LSCC lung tumors. We developed a small molecule that inhibits  
8 USP28 activity in the low nanomole range. While displaying cross-reactivity against  
9 the closest homologue USP25, this inhibitor showed a high degree of selectivity over  
10 other deubiquitinases. USP28 inhibitor treatment resulted in a dramatic decrease in c-  
11 Myc proteins levels and consequently induced substantial regression of  
12 autochthonous murine LSCC tumors and human LSCC xenografts, thereby  
13 phenocopying the effect observed by genetic deletion. Thus, USP28 may represent a  
14 promising therapeutic target for the treatment of squamous cell lung carcinoma.

15

## 1 **Introduction**

2 Lung cancer is the leading cause of cancer death worldwide. Based on histological  
3 criteria lung cancer can be subdivided into non-small cell lung cancer (NSCLC) and  
4 the rarer small cell lung cancer. The most common NSCLCs are lung adenocarcinoma  
5 (LADC) and squamous cell carcinoma (LSCC), with large cell carcinoma being less  
6 commonly observed. Progress has been made in the targeted treatment of LADC,  
7 largely due to the development of small-molecule inhibitors against EGFR, ALK, and  
8 ROS1 (Cardarella and Johnson, 2013). However, no targeted treatment options exist  
9 for LSCC patients (Hirsch et al., 2017; Novello et al., 2014). Consequently, despite  
10 having limited efficacy on LSCC patient survival, platinum-based chemotherapy  
11 remains the cornerstone of current LSCC treatment (Fennell et al., 2016; Isaka et al.,  
12 2017; Scagliotti et al., 2008). Therefore, there is an urgent need to identify novel  
13 druggable targets for LSCC treatment and to develop novel therapeutics.

14 The *FBXW7* protein product F-box/WD repeat-containing protein 7 (FBW7) is the  
15 substrate recognition component of an SCF-type ubiquitin ligase, which targets  
16 several well-known oncoproteins, including c-Myc, Notch, and c-Jun, for degradation  
17 (Davis et al., 2014). These oncoproteins accumulate in the absence of FBW7 function,  
18 and genetic analyses of human LSCC samples revealed common genomic alterations  
19 in *FBXW7* (Cancer Genome Atlas Research, 2012; Kan et al., 2010). In addition,  
20 FBW7 protein is undetectable by immunohistochemistry (IHC) in 69% of LSCC patient  
21 tumor samples (Ruiz et al., 2019). Genetically engineered mice harboring loss of  
22 *Fbxw7* concomitant with *KRasG12D* activation (KF mice) develop LSCC with 100%  
23 penetrance and short latency, as well as LADC (Ruiz et al., 2019). Thus, FBW7 is an  
24 important tumor suppressor in both human and murine lung cancer.

1 The deubiquitinase USP28 opposes FBW7-mediated ubiquitination of the  
2 oncoproteins c-Myc and c-Jun, thereby stabilizing these proteins (Popov et al., 2007).

3 In a murine model of colorectal cancer, deleting *Usp28* reduced size of established  
4 tumors and increased lifespan (Diefenbacher et al., 2014). Therefore, targeting USP28  
5 in order to destabilize its substrates represents an attractive strategy to inhibit the  
6 function of c-Myc and other oncogenic transcription factors that are not amenable to  
7 conventional inhibition by small molecules.

8 Here, we describe the characterisation of a novel USP28 inhibitory compound  
9 (USP28i) and the genetic as well as chemical validation of USP28 as a promising  
10 therapeutic target for LSCC tumors. Using an FRT/FLP and CRE/LOXP dual  
11 recombinase system (Schonhuber et al., 2014), we show that *Usp28* inactivation in  
12 established LSCC results in dramatic tumor regression. Importantly, USP28i treatment  
13 recapitulates LSCC regression in both mouse models and human LSCC xenografts.  
14 Absence or inhibition of USP28 resulted in a dramatic decrease in the protein levels  
15 of c-Myc, providing a potential mechanism of action for USP28i. Therefore, USP28  
16 inhibition should be a strong candidate for clinical evaluation, particularly given the  
17 paucity of currently available therapy options for LSCC patients.

18

19

## 1 Results

### 2 **USP28 is required to maintain protein levels of c-Myc, c-Jun and $\Delta$ p63 in LSCC**

3 To gain insights into the molecular differences between LADC and LSCC, we  
4 investigated the expression of MYC in these common NSCLCs subtypes. MYC was  
5 transcriptionally upregulated in human LSCC compared to healthy lung tissue or  
6 LADC tumors (**Figure 1A**). Quantitative polymerase chain reaction (qPCR) analysis  
7 on an independent set of primary human lung biopsy samples confirmed that MYC is  
8 highly expressed in LSCC tumors compared with normal lung tissue (**Figure 1B**).  
9 Moreover, immunohistochemistry (IHC) staining on primary lung tumors confirmed a  
10 significant abundance of c-Myc protein in LSCC samples (**Figure 1C, 1D**). Also  $\Delta$ p63  
11 and c-Jun, critical factors in squamous cell identity and tumor maintenance,  
12 respectively, showed higher protein levels in LSCC compared to LADC tumors (**Figure**  
13 **1C, 1D**). Individual downregulation of c-Myc, c-Jun and  $\Delta$ p63 by siRNA resulted in a  
14 significant reduction of cell growth in four independent human LSCC cell lines (**Figure**  
15 **1E, S1A-C**).

16 As c-Myc, c-Jun and  $\Delta$ p63 protein levels are controlled by the deubiquitinase USP28  
17 (Popov et al., 2007; Prieto-Garcia et al., 2020), we analysed its expression in publicly  
18 available datasets (The Cancer Genome Atlas). We observed that 25% of human  
19 LSCC cases show gain-of-function alterations in *USP28* (**Figure 1F**). In addition, a  
20 positive correlation between *USP28* copy-number and mRNA expression was found  
21 in the same datasets (**Figure S2A**). Interestingly, qPCR and IHC analysis on human  
22 LSCC samples revealed that low *USP28* mRNA levels correlated with low USP28  
23 protein levels and likewise, high/moderate mRNA levels also correlated with high  
24 USP28 protein levels (**Figure 1G, S2B**). Since USP28 is involved in  $\Delta$ p63, c-Jun and  
25 c-Myc stabilization and higher expression of USP28 is associated with a significantly

1 shorter survival time (Prieto-Garcia et al., 2020), we targeted its expression. Usp28  
2 downregulation by shRNA resulted in a significant reduction in c-Myc, c-Jun and  $\Delta$ p63  
3 protein levels in LSCC primary tumor cells and reduced LSCC cell growth (**Figure 1H,**  
4 **1I**). Thus, targeting USP28 in order to destabilize its substrates represents a rational  
5 strategy to target tumor cells that rely on oncogenic transcription factors that are  
6 currently not druggable by small molecules.

7

### 8 **Generation of a pre-clinical dual recombinase lung cancer mouse model**

9 Recently, Usp28 was shown to be required for the initiation of lung tumors in the  
10 Rosa26-Cas9 sgRNA Kras<sup>G12D</sup>; Tp53; Lkb1 model (Prieto-Garcia et al., 2020).  
11 However, a meaningful pre-clinical model requires targeting the therapeutic candidate  
12 gene in existing growing lung tumors. Thus, to assess the function of *Usp28* in  
13 established tumors, we developed a new genetically engineered mouse (GEM) model  
14 to temporally and spatially separate tumor development from target deletion by using  
15 two independent recombinases: Flp and Cre<sup>ERT</sup>. In this model, LSCC and LADC  
16 formation is initiated by KRas<sup>G12D</sup> activation and *Fbxw7* deletion using Flp  
17 recombinase, and the Cre/loxP system can then be used for inactivation of Usp28<sup>flx/flx</sup>  
18 in established tumors. To allow conditional FRT/Flp-mediated inactivation of *Fbxw7*  
19 function, we inserted two FRT sites flanking exon 5 of the endogenous *Fbxw7* gene in  
20 mice to generate a Fbxw7<sup>FRT/FRT</sup> allele that can be deleted by Flp recombinase (**Figure**  
21 **S3A, S3B**). Expression of Flp recombinase resulted in the deletion of *Fbxw7* exon 5,  
22 which could be detected by PCR (**Figure S3B**). The resulting strain, Fbxw7<sup>FRT/FRT</sup>,  
23 was crossed to FRT-STOP-FRT (FSF)-KRas<sup>G12D</sup> mice to generate FSF-KRas<sup>G12D</sup>;  
24 Fbxw7<sup>FRT/FRT</sup> (KF-Flp model).

25

## 1 **USP28 is an effective therapeutic target for LSCC, but not KRas<sup>G12D</sup>; Trp53** 2 **mutant LADC tumors**

3 The KF-Flp strain described above was crossed with ROSA26-FSF-Cre<sup>ERT</sup>;  
4 *Usp28*<sup>flox/flox</sup> mice to generate the KFCU model (**Figure 2A**). KFCU tumor development  
5 was monitored by CT scans. At ten-to-eleven weeks post-infection with Flp  
6 recombinase-expressing recombinant adenoviruses, animals displayed lesions in  
7 their lungs. At this time point, we confirmed by histology that KFCU mice develop both  
8 LADC and LSCC tumors (**Figure S3C**). As expected (Ruiz et al., 2019), KFCU LADC  
9 lesions occurred in alveolar tissue and were positive for Sftpc and TTF1. KFCU LSCC  
10 tumors occurred mainly in bronchi (rarely manifesting in the alveolar compartment)  
11 and expressed CK5 and  $\Delta p63$ . Next, animals displaying lung tumors were exposed to  
12 tamoxifen to activate the Cre<sup>ERT</sup> protein and delete the conditional *Usp28* floxed alleles  
13 (**Figure 2A, S3D**). Although the loss of *Usp28* expression decreased LADC tumor  
14 size, it did not reduce the number of LADC tumors (**Figure 2B-D**). In contrast,  
15 histological examination of KFCU mice revealed a clear reduction in the numbers of  
16 LSCC lesions in *Usp28*-deleted lungs (**Figure 2F, S3D**). As well as a significant  
17 reduction in tumor number, the few CK5-positive LSCC lesions that remained were  
18 substantially smaller than control tumors (**Figure 2G**). Measurement of the size of 429  
19 individual KFCU LSCC tumors (326 vehicle-treated and 103 tamoxifen-treated)  
20 showed an average size of  $11.4 \times 10^4 \mu\text{m}^2$  in the vehicle arm versus  $4.6 \times 10^4 \mu\text{m}^2$  in the  
21 tamoxifen arm (**Figure 2G**). Thus, *Usp28* inactivation significantly reduces both the  
22 number and the size of LSCC tumors.

23 To get insights into LSCC tumor regression, we focused on *Usp28* substrates.  
24 Immunoblotting analysis revealed that *Usp28* deletion resulted in apoptotic cell death  
25 (cleaved caspase-3; CC3).  $\Delta p63$  protein levels were reduced, but c-Jun and c-Myc



1 protein became undetectable (**Figure 2H, S3E**). *Usp28* deletion also decreased c-Jun  
2 and c-Myc levels in KFCU LADC lesions, although the reduction in c-Myc protein levels  
3 were significantly less pronounced than observed in LSCC (**Figure 2E**). Strikingly,  
4 elimination of *Usp28* has little effect, if any, on apoptotic cell death, as determined by  
5 its inability to induce cleaved caspase-3 in LADC lesions. Thus, these data suggest  
6 that *Usp28* and its substrates are required for the maintenance of LSCC tumors.  
7 To further investigate the role of *Usp28* in LADC, we studied the consequences of  
8 *Usp28* deletion in a second LADC genetic model. We used Flp-inducible oncogenic  
9 K-Ras activation combined with p53 deletion (FSF-KRas<sup>G12D</sup> and Trp53<sup>FRT/FRT</sup> or KP-  
10 Flp model) (Schonhuber et al., 2014). The KP-Flp mice were crossed to a conditional  
11 *Usp28*<sup>flox/flox</sup> strain together with an inducible Cre<sup>ERT</sup> recombinase knocked in at the  
12 ROSA26 locus and an mT/mG reporter allele (KPCU mice; **Figure 3A**). After  
13 intratracheal adeno-CMV-Flp virus instillation, *Usp28* was deleted in KPCU animals  
14 displaying lung tumors by CT (**Figure 3A**). Loss of *Usp28* expression in this second  
15 LADC model also did not result in a reduction of LADC tumor number and size (**Figure**  
16 **3C, 3D**). Successful Cre<sup>ERT</sup> recombination was verified using lineage tracing (GFP  
17 staining) and deletion of *Usp28*<sup>flox/flox</sup> alleles was further confirmed by BaseScope  
18 assays (**Figure 3B, 3E**). Therefore, also these data argue against an important role  
19 for *Usp28* in LADC tumors.

20

## 21 **Generation of a new USP28 inhibitor: selectivity and cellular target engagement**

22 The finding that *Usp28* plays a key role in LSCC tumor maintenance prompted us to  
23 identify small molecule inhibitors against this deubiquitinase. A small molecule  
24 discovery campaign based on the ubiquitin-rhodamine cleavable assay (Turnbull et  
25 al., 2017) yielded a panel of compounds sharing a thienopyridine carboxamide

1 chemical scaffold with inhibitory selectivity for USP28 and USP25 (Guerin, 2017;  
2 Guerin et al., 2020; Zablocki et al., 2019). The compound FT206 (**Figure 4A**)  
3 represents a different chemical class from the benzylic amino ethanol-based inhibitors  
4 described previously (Wrigley et al., 2017). Quantitative structure-activity relationship  
5 (SAR) was used to develop compound derivative FT206 that was most optimal in  
6 terms of drug metabolism and pharmacokinetic properties (DMPK) while preserving  
7 potency and selectivity towards USP28/25 (Zablocki et al., 2019). To confirm FT206  
8 cellular target engagement, we used a Ub activity-based probe assay (ABP) (Altun et  
9 al., 2011; Clancy et al., 2021; Panyain et al., 2020; Turnbull et al., 2017). ABPs can  
10 assess DUB enzyme activity in a cellular context. DUB inhibition leads to displacement  
11 of the ABP probe, resulting in a molecular weight shift measurable by SDS-PAGE and  
12 immunoblotting against USP28/25. Using this approach, we found that the compound  
13 FT206 interferes with USP28/25 probe labelling (USP-ABP versus USP) in LSCC  
14 H520 cell extracts ( $EC_{50}$  ~300-1000nM, **Figure 4B**) and intact cells ( $EC_{50}$  ~1-3 $\mu$ M,  
15 **Figure 4C**). In contrast to FT206, AZ1, a different USP28 inhibitor (Wrigley et al.,  
16 2017), based on a benzylic amino ethanol scaffold, appeared to exert lower potency  
17 towards USP28 ( $EC_{50}$  >30 $\mu$ M) and selectivity for USP25 ( $EC_{50}$  ~10-30 $\mu$ M) (**Figure**  
18 **S4A**). To address compound selectivity more widely, we combined the ABP assay  
19 with quantitative mass spectrometry (ABPP) to allow the analysis of the cellular active  
20 DUBome (Benns et al., 2021; Jones et al., 2021; Pinto-Fernandez et al., 2019). When  
21 performing such assay in human LSCC cells, we were able to profile 28 endogenous  
22 DUBs, revealing a remarkable USP28/25 selectivity for FT206 in a dose-dependent  
23 manner (**Figure 4D**).

24 To further evaluate the efficacy of FT206 in targeting USP28, we tested its ability to  
25 modulate the ubiquitination status of endogenous USP28 substrates. The

1 ubiquitination levels of c-Myc and c-Jun increased upon FT206 and MG132 co-  
2 treatment (**Figure 4SB**), confirming that FT206 blocks USP28-mediated  
3 deubiquitination of its substrates. The ubiquitination level of USP28 also increased  
4 upon FT206 treatment (**Figure 4SB**), which is consistent with previous observations  
5 where the enzymatic activity of DUBs can function to enhance their own stability (de  
6 Bie and Ciechanover, 2011). Consequently, treatment of LSCC tumor cells with FT206  
7 resulted in reduced c-Myc, c-Jun,  $\Delta p63$  and Usp28 protein levels, which were restored  
8 upon addition of MG132 (**Figure 4E, S4C**).  
9 Finally, FT206 treatment impaired LSCC cell growth (**Figure 4F**). However, in a  
10 USP28-depleted background, FT206 neither affected cell growth nor reduced c-Myc  
11 protein levels (**Figure S4D**). Thus, this data suggests that the effects of FT206 are  
12 mediated by USP28.

13

#### 14 **Pharmacological inhibition of USP28 is well tolerated in mice and induced LSCC** 15 **tumor regression**

16 We next evaluated the therapeutic potential of the USP28 inhibitor FT206 using the  
17 LSL-KRas<sup>G12D</sup>; Fbxw7<sup>flox/flox</sup> model (KF mice), which develop both LADC and LSCC  
18 tumor types (Ruiz et al., 2019). Nine weeks after adeno-CMV-Cre virus infection, when  
19 mice had developed lung tumors, we started treatment with USP28 inhibitor at 75  
20 mg/kg, 3 times a week for 5 weeks (**Figure 5A**). FT206 administration had no  
21 noticeable adverse effects and treated mice maintained normal body weight (**Figure**  
22 **S5A, S5B**). Consistent with the effects observed by genetic *Usp28* inactivation  
23 (**Figure 2C**), the number of KF LADC lesions was not affected by Usp28 inhibition via  
24 FT206 treatment (**Figure 5B, 5C, 5D**). By contrast, we found that FT206 effectively  
25 reduced LSCC tumor number by 68% (31 to 10 LSCC tumors, **Figure 5B, 5E**).

1 Moreover, measurement of 252 individual KF LSCC mutant tumors (156 vehicle-  
2 treated and 96 FT206-treated lesions) showed a significant reduction of over 45% in  
3 tumor size upon FT206 treatment: an average of  $8.5 \times 10^4 \mu\text{m}^2$  in the vehicle arm versus  
4  $4.5 \times 10^4 \mu\text{m}^2$  in the FT206 cohort (**Figure 5F**). Thus, Usp28 inhibition by FT206 leads  
5 to a dramatic reduction in the numbers of advanced LSCC tumors, and the small  
6 number of remaining LSCC lesions are significantly reduced in size, resulting in a  
7 reduction of total LSCC burden of over 85% by single agent treatment.

8 In line with the effects found by genetic *Usp28* deletion, treatment of KF mice with  
9 FT206 also resulted in reduced  $\Delta\text{p63}$ , c-Jun and c-Myc protein levels (**Figure 5G**).  
10 Consequently, FT206 treatment led to a substantial increase in the number of cleaved  
11 caspase-3-positive cells in LSCC while LADC cells were not significantly affected,  
12 indicating that Usp28 inhibition causes apoptotic cell death of LSCC tumor cells  
13 (**Figure 5H, 5I**).

14 Finally, to further confirm the specificity of FT206, KFCU mice pre-exposed to  
15 tamoxifen to delete the conditional *Usp28* floxed alleles were further treated with the  
16 USP28 inhibitor FT206. In this setting, Usp28 inhibition did not result in a further  
17 reduction of LADC and LSCC lesions (**Figure 2C, 2F**), suggesting that FT206 targets  
18 specifically Usp28.

19

## 20 **USP28 inhibition causes dramatic regression of human LSCC xenograft tumors**

21 To determine whether the promise of USP28 as a target in mouse lung cancer models  
22 can be translated to a human scenario, we established human xenograft tumor  
23 models. siRNA-mediated *USP28* depletion, and USP28 inhibitor treatment,  
24 considerably reduced protein levels of  $\Delta\text{p63}$ , c-Jun and c-Myc and impaired growth in  
25 human LSCC tumor cells (**Figure 6A-C, S6A**). In contrast, FT206 treatment had

1 marginal effects on c-Myc and c-Jun protein levels in human LADC cells (**Figure S6B**).  
2 Crucially, FT206 led to a remarkable growth impairment of xenografts derived from  
3 three independent human LSCC cell lines (**Figure 6D-I**), which was accompanied with  
4 a strong reduction of c-Myc protein levels (**Figure 6J-L**). In summary, these data  
5 suggest that USP28 pharmacological intervention is a promising therapeutic option for  
6 human LSCC patients.

## 1 **Discussion**

2 Unlike for LADC, there are few approved targeted therapies against LSCC.  
3 Consequently, despite its limited effectiveness on disease progression and prognosis,  
4 patients with LSCC receive the same conventional platinum-based chemotherapy  
5 today as they would have received two decades ago (Fennell et al., 2016; Gandara et  
6 al., 2015; Isaka et al., 2017; Liao et al., 2012; Scagliotti et al., 2008).

7 c-MYC is a transcription factor that orchestrates a potent pro-cancer programme  
8 across multiple cellular pathways. As c-MYC is often overexpressed in late-stage  
9 cancer, targeting it for degradation is an attractive strategy in many settings. The term  
10 'undruggable' was coined to describe proteins that could not be targeted  
11 pharmacologically. Many desirable targets in cancer fall into this category, including  
12 the c-MYC oncoprotein, and pharmacologically targeting these intractable proteins is  
13 a key challenge in cancer research.

14 The deubiquitylase family of enzymes have emerged as attractive drug targets, that  
15 can offer a means to destabilize client proteins that might otherwise be undruggable  
16 (Schauer et al., 2019). The deubiquitinase USP28 was known to remove FBW7-  
17 mediated ubiquitination of, and thereby stabilise, the oncoprotein c-MYC (Popov et al.,  
18 2007). Importantly, mice lacking *Usp28* are healthy (Knobel et al., 2014), suggesting  
19 that *Usp28* is dispensable for normal physiology and homeostasis.

20 In the current study we identified a requirement for USP28 for the maintenance of  
21 murine and human LSCC tumors. In agreement with the absence of major phenotypes  
22 in the *Usp28* knock out mice, USP28 inhibitor treatment was well tolerated by the  
23 experimental animals, while having a dramatic effect on LSCC regression. USP28  
24 small molecule inhibition phenocopies the effects of *Usp28* deletion in LSCC  
25 regression, consistent with on-target activity. However, we cannot exclude that the

1 inhibition of USP25 and possibly additional off-targets effects may contribute to the  
2 observed phenotype. Inhibitor treated mice kept a normal body weight, indicating no  
3 global adverse effects (**Figure S5A**).

4 While USP28 inhibition resulted in profoundly reduced LSCC growth, the effect on  
5 LADC was modest. TP63, c-Jun and c-Myc protein levels are increased in LSCC  
6 compared to LADC (**Figure 1C, 1D**). This could indicate a greater dependence of  
7 LSCC on these oncoproteins, which consequently may result in increased sensitivity  
8 to USP28 inhibition. We previously found that *Usp28* deficiency corrected the  
9 accumulation of SCF (Fbw7) substrate proteins, including c-Jun and c-Myc, in *Fbw7*-  
10 mutant cells (Diefenbacher et al., 2015). The frequent downregulation of *FBXW7* in  
11 human LSCC (Ruiz et al., 2019) (**Figure S2B**) may underlie the increased  
12 accumulation of SCF(Fbw7) substrate proteins like c-Myc, c-Jun and p63 in LSCC,  
13 and thereby cause LSCC tumors to be increasingly dependent on USP28 function.  
14 Indeed, our study suggest that those 3 oncoproteins are all relevant targets of USP28  
15 in LSCC (**Figure 2H**). In contrast, Prieto-Garcia et al. saw no difference in c-Jun and  
16 c-Myc protein levels, and suggested a different mechanism of action. Of note, our and  
17 the Prieto-Garcia et al. studies used different dual specificity inhibitors of USP28/25  
18 that have distinct properties. FT206, the compound used in this study, preferentially  
19 inhibits USP28 compared to USP25, whereas AZ1, the compound used by Prieto-  
20 Garcia et al. showed a pronounced activity towards USP25. In addition, FT206 inhibits  
21 USP28 in the nano-molar range, while Prieto-Garcia et al. typically used AZ1 at 10-  
22 30 $\mu$ M, possibly because higher compound concentrations are required for therapeutic  
23 inhibition of USP28. Therefore differences in the selectivity and potency of the  
24 compounds used may explain some of the differences observed.

1 Interestingly, all human LSCC cell lines used in the xenograft experiment (**Figure 6**),  
2 each of which responded well to USP28 inhibition, do not show neither gain- or loss-  
3 of-function mutations in *USP28* nor *FBXW7*, respectively. Thus, these data support  
4 the notion that LSCC tumor cells respond to USP28 inhibition, regardless of  
5 *USP28/FBXW7* mutation status, which suggest that USP28 inhibition might be a  
6 therapeutic option for many LSCC patients.

7 In summary, our studies demonstrate that USP28 is a key mediator of LSCC  
8 maintenance and progression and hence USP28 represents an exciting therapeutic  
9 target. Therefore, USP28 inhibition should be considered as a potential therapy for  
10 human lung squamous cell carcinoma.

11



## 1 **Methods and Materials**

2

### 3 **Mice**

4 The LSL-KRas<sup>G12D</sup> (Jackson et al., 2001), Fbxw7<sup>flox/flox</sup> (Jandke et al., 2011),  
5 Usp28<sup>flox/flox</sup> (Diefenbacher et al., 2014), FSF-KRas<sup>G12D</sup> (Schonhuber et al., 2014),  
6 Trp53<sup>FRT/FRT</sup> (Schonhuber et al., 2014), ROSA26-FSF-Cre<sup>ERT</sup> (Schonhuber et al.,  
7 2014), ROSA26-LSL-mTmG (Muzumdar et al., 2007) strains have been previously  
8 described. Immunocompromised NSG mice were maintained in-house. All animal  
9 experiments were approved by the Francis Crick Institute Animal Ethics Committee  
10 and conformed to UK Home Office regulations under the Animals (Scientific  
11 Procedures) Act 1986 including Amendment Regulations 2012. All strains were  
12 genotyped by Transnetyx. Each group contained at least 3 mice, which generates  
13 enough power to pick up statistically significant differences between treatments, as  
14 determined from previous experience (Ruiz et al., 2019). Mice were assigned to  
15 random groups before treatment.

16

### 17 **Generation of Fbxw7<sup>FRT/FRT</sup> Mice**

18 To generate a conditional allele of Fbxw7, we employed the CRISPR-Cas9 approach  
19 to insert two FRT sites into the intron 4 and 5 of Fbxw7, respectively. Two guide RNAs  
20 targeting the integration sites (gRNA-Int5A: accgtcggcacactggtcca; gRNA-Int4A:  
21 cactcgtcactgacatcgat), two homology templates containing the FRT sequences  
22 (gRNA-Int5B: agcactgacgagtgaggcgg; gRNA-Int4B: tgctagccttttacaagat) and the  
23 Cas9 protein were micro-injected into the fertilised mouse eggs. The offspring were  
24 screened by PCR and one line with proper integration of two FRT sites was identified.

25

26

## 1 **Analysis of public data from cancer genomics studies**

2 Data from TCGA Research Network (Lung Squamous Cell Carcinoma (TCGA,  
3 Firehose Legacy)), including mutations, putative copy-number alterations, and mRNA  
4 Expression (mRNA expression z-scores relative to diploid samples (RNA Seq V2  
5 RSEM; threshold 2.0), were analyzed using cBioportal software and visualized using  
6 the standard Oncoprint output (Cerami et al., 2012). The Onco Query Language (OQL)  
7 used was “USP28: MUT AMP GAIN EXP >= 2” “FBXW7: MUT HOMDEL  
8 HETLOSS EXP <= -2”. Source data was from GDAC Firehose, previously known as  
9 TCGA Provisional. The complete sample set used was (n = 178). Expression analysis  
10 was performed using GEPIA (Gene expression profiling interactive analysis) software  
11 (2017).

12

## 13 **Human lung tumor analysis**

14 Human biological samples were collected, stored, and managed by the Cordoba node  
15 belonging to the Biobank of the Andalusian Health Service (Servicio Andaluz de Salud-  
16 SAS) and approved by the Ethics and Clinical Research Committee of the University  
17 Hospital Reina Sofia. All subjects gave informed consent. Pathologists assessed all  
18 samples before use. mRNA extracted from the samples was analyzed by qPCR.  
19 Primers are listed in Table 1.

20

## 21 **Tumor induction and tamoxifen treatment**

22 Induction of NSCLC tumors was carried out in anesthetized (2-2.5% isoflurane) mice  
23 by intratracheal instillation of a single dose of  $2.5 \times 10^7$  pfu of adenoviruses encoding  
24 either the Cre recombinase (adeno-CMV-Cre) or Flp recombinase (adeno-CMV-Flp).

1 Activation of the inducible Cre<sup>ERT2</sup> recombinase was carried out by intraperitoneal  
2 injection of tamoxifen (100 µg/kg body weight) dissolved in peanut oil for 10 days.

3

#### 4 **CT image acquisition and processing**

5 The SkyScan-1176, a high-resolution low-dose X-ray scanner, was used for 3D  
6 computed tomography (CT). Mice were anesthetized with 2-2.5% isoflurane and CT  
7 images were acquired at a standard resolution (35 µm pixel size). The raw scan data  
8 was sorted using RespGate software, based on the position of the diaphragm, into  
9 end expiration bins. 3D reconstruction was performed using NRecon software. 3D  
10 data sets were examined using Data Viewer software.

11

#### 12 **Mouse treatments with FT206**

13 Nine-weeks upon Ad5-CMV-Cre infection, LSL-KRas<sup>G12D</sup>; Fbxw7<sup>flox/flox</sup> mice were  
14 treated with FT206 (75 mg/kg) via oral gavage on day 1, 3, and 5 per week during 5  
15 weeks. Body weights were register every week.

16

#### 17 **In vivo pharmacology with subcutaneous graft tumors**

18 Human LSCC tumor cell lines (NCI-H520, CALU-1 and LUDLU-1) were resuspended  
19 as single-cell suspensions at 10<sup>7</sup> cells/ml in PBS:Matrigel. 100 µl (10<sup>6</sup> cells total) of  
20 this suspension was injected into the flanks of immunodeficient NSG mice. When  
21 tumors were palpable, treatment with FT206 (75 mg/kg) was initiated with the same  
22 schedule on day 1, 3, and 5 per week. Tumor grafts were measured with digital  
23 callipers, and tumor volumes were determined with the following formula: (length ×  
24 width<sup>2</sup>) × (π/6). Tumor volumes are plotted as means ± SD.

25

## 1 **Histopathology, Immunohistochemistry and BaseScope analysis**

2 For histological analysis, lungs were fixed overnight in 10% neutral buffered formalin.

3 Fixed tissues were subsequently dehydrated and embedded in paraffin, and sections

4 (4  $\mu\text{m}$ ) were prepared for H&E staining or IHC. Antibodies are given in Table 2.

5 BaseScope was performed following the manufacturer's protocol. The *Usp28*-specific

6 probe was custom-designed to target 436-482 of NM\_175482.3; *Ppib* probe was used

7 as a positive control (Bio-Techne Ltd).

8 Tumor numbers were counted from whole lung sections: LADC and LSCC tumors

9 were identified by Sftpc and CK5 stains, respectively. Tumor areas ( $\mu\text{m}^2$ ) were

10 measured from lung sections using Zen3.0 (blue edition) software. For quantification

11 of tumor cell death, the number of cleaved caspase-3-positive cells was counted in

12 individual tumors per field (20x). The number of  $\Delta\text{p63}^+$ , c-Myc<sup>+</sup> and c-Jun<sup>+</sup> cells was

13 counted in individual tumors/10,000 $\mu\text{m}^2$ . All analyses were performed uniformly

14 across all lung sections and the whole lungs were used to derive data.

15

## 16 **Cell culture**

17 Primary KF LSCC cells were cultured in N2B27 medium containing EGF (10 ng/ml;

18 Pepro Tech) and FGF2 (20 ng/ml; Pepro Tech) (Ruiz et al., 2019). Human lung

19 squamous cell carcinoma (NCI-H226, NCI-H520, CALU-1 and LUDLU-1) and lung

20 adenocarcinoma (NCI-H23, NCI-H441 and NCI-H1650) lines were provided by the

21 Francis Crick Institute Cell Services and cultured in RPMI-1640 medium

22 supplemented with 10% FBS, 1% penicillin/streptomycin, 2mM Glutamine, 1% NEEA

23 and 1mM Na Pyruvate. All cells were tested Mycoplasma negative and maintained at

24 37°C with 5% CO<sub>2</sub>.

25

## 1 **Cell treatments**

2 Mouse KF LSCC and human LUDLU-1 cells were treated with vehicle or FT206 at  
3 different concentrations for 48hr to analyse c-Myc, c-Jun and  $\Delta$ p63 protein levels by  
4 western-blotting.

5 Primary mouse KF LSCC cells were infected with inducible-shRNAs against the  
6 Usp28 gene and then expose to Doxycycline hyclate (1 $\mu$ g/ml) for 48h. Cell number  
7 was counted using an automated cell counter (Thermo Fisher Scientific, Countess  
8 Automated Cell Counter).

9 Mouse KF LSCC and human cell lines were transfected with specific small interfering  
10 RNAs (siRNAs) against the *MYC*, *JUN*, *TP63* or *USP28* genes, using Lipofectamine  
11 RNAiMAX and 25nM of each siRNA according to the manufacturer's instructions  
12 (Dharmacon). 72-96h later, cell number was counted using an automated cell counter.

13 For IC<sub>50</sub>, mouse KF LSCC and human cells were treated with vehicle or FT206 at  
14 different concentrations for 72h. Cell viability was measured as the intracellular ATP  
15 content using the CellTiter-Glo Luminescent Cell Viability Assay (Promega), following  
16 the manufacturer's instructions. IC<sub>50</sub> was calculated using GraphPad Prism software.

17

## 18 **Western Blot Analysis**

19 Cells were lysed in ice-cold lysis buffer (20 mM Tris HCl, pH 7.5, 5 mM MgCl<sub>2</sub>, 50 mM  
20 NaF, 10 mM EDTA, 0.5 M NaCl, and 1% Triton X-100) that was completed with  
21 protease, phosphatase, and kinase inhibitors. Protein extracts were separated on  
22 SDS/PAGE gel, transferred to a nitrocellulose membrane and blotted with antibodies  
23 are given in Table 2. Primary antibodies were detected against mouse or rabbit IgGs  
24 and visualized with ECL Western blot detection solution (GE Healthcare) or Odyssey  
25 infrared imaging system (LI-COR, Biosciences).

## 1 **USP28 inhibitor synthesis**

2 Synthesis and characterization of the USP28/25 small molecule inhibitor FT206, a  
3 thienopyridine carboxamide derivative, has been described previously in the patent  
4 application WO 2017/139778 A1 (Guerin, 2017) and more recent updates WO  
5 2019/032863 (Zablocki et al., 2019) and WO 2020/033707 (Guerin et al., 2020), where  
6 FT206 is explicitly disclosed as Example 11.1.

7

## 8 **Cellular DUB profiling using Ub-based active site directed probes**

9 Molecular probes based on the ubiquitin scaffold were generated and used essentially  
10 as described (Pinto-Fernandez et al., 2019; Turnbull et al., 2017). In brief, HA-tagged  
11 Ub propargyl probes were synthesised by expressing the fusion protein HA-Ub75-  
12 Intein-Chitin binding domain in E.Coli BL21 strains. Bacterial lysates were prepared  
13 and the fusion protein purified over a chitin binding column (NEB labs, UK). HA-Ub75-  
14 thioester was obtained by incubating the column material with mercaptosulfonate  
15 sodium salt (MESNa) overnight at 37°C. HA-Ub75-thioester was concentrated to a  
16 concentration of ~1 mg/ml using 3,000 MW filters (Sartorius) and then desalted against  
17 PBS using a PD10 column (GE Healthcare). 500 µL of 1-2 mg/mL of HA-Ub75-  
18 thioester was incubated with 0.2 mmol of bromo-ethylamine at pH 8-9 for 20 minutes  
19 at ambient temperature, followed by a desalting step against phosphate buffer pH 8  
20 as described above. Ub probe material was concentrated to ~1mg/ml, using 3,000  
21 MW filters (Sartorius), and kept as aliquots at -80°C until use.

22

## 23 **DUB profiling competition assays with cell extracts and with cells**

24 Crude NCI-H520 cell extracts were prepared as described previously using glass-  
25 bead lysis in 50 mM Tris pH 7.4, 5 mM MgCl<sub>2</sub>, 0.5 mM EDTA, 250 mM sucrose, 1 mM

1 DTT. For experiments with crude cell extracts, 50 µg of NCI-H520 cell lysate was  
2 incubated with different concentrations of USP28 inhibitor compounds (FT206 and  
3 AZ1) for one hour at 37 °C, followed by addition of 1 µg HA-UbPA and incubation for  
4 10 minutes (Figure 4B, 4C) or 30 minutes (Figure S4A comparing FT206 and AZ1) at  
5 37 °C. Incubation with Ub-probe was optimised to minimise replacement of non-  
6 covalent inhibitor FT206 by the covalent probe. Samples were then subsequently  
7 boiled in reducing SDS-sample buffer, separated by SDS-PAGE and analysed by  
8 Western Blotting using anti-HA (Roche, 1:2000), anti-USP28 (Abcam, 1:1000), anti-  
9 USP25 (Abcam, 1:1000), anti-GAPDH (Invitrogen, 1:1000) or beta Actin (Abcam,  
10 1:2000) antibodies. For cell-based DUB profiling,  $5 \times 10^6$  intact cells were incubated  
11 with different concentrations of inhibitors in cultured medium for 4 hours at 37 °C,  
12 followed by glass-bead lysis, labelling with HA-UbPA probe, separation by SDS-PAGE  
13 and Western blotting as described above.

14

### 15 **DUB inhibitor profiling by quantitative mass spectrometry**

16 Ub-probe pulldown experiments in presence of different concentrations of the inhibitor  
17 FT206 were performed essentially as described (Pinto-Fernandez et al., 2019;  
18 Turnbull et al., 2017) with some modifications. In brief, immune precipitated material  
19 from 500 µg-1 mg of NCI-H520 cell crude extract was subjected to in-solution trypsin  
20 digestion and desalted using C18 SepPak cartridges (Waters) based on the  
21 manufacturer's instructions. Digested samples were analyzed by nano-UPLC-MS/MS  
22 using a Dionex Ultimate 3000 nano UPLC with EASY spray column (75 µm x 500 mm,  
23 2 µm particle size, Thermo Scientific) with a 60 minute gradient of 0.1% formic acid in  
24 5% DMSO to 0.1% formic acid to 35% acetonitrile in 5% DMSO at a flow rate of ~250  
25 nl/min (~600 bar/40 °C column temperature). MS data was acquired with an Orbitrap

1 Q Exactive High Field (HF) instrument in which survey scans were acquired at a  
2 resolution of 60.000 at 400 m/z and the 20 most abundant precursors were selected  
3 for CID fragmentation. From raw MS files, peak list files were generated with  
4 MSConvert (Proteowizard V3.0.5211) using the 200 most abundant peaks/spectrum.  
5 The Mascot (V2.3, Matrix Science) search engine was used for protein identification  
6 at a false discovery rate of 1%, mass deviation of 10 ppm for MS1 and 0.06 Da (Q  
7 Exactive HF) for MS2 spectra, cys carbamidylation as fixed modification, met oxidation  
8 and Gln deamidation as variable modification. Searches were performed against the  
9 UniProtKB human sequence data base (retrieved 15.10.2014). Label-free quantitation  
10 was performed using MaxQuant Software (version 1.5.3.8), and data further analysed  
11 using GraphPad Prism software (v7) and Microsoft Excel. Statistical test-s ANOVA  
12 (multiple comparison; Original FDR method of Benjamini and Hochberg) was  
13 performed using GraphPad Prism software. The MS data was submitted to PRIDE for  
14 public repository with an internal ID of px-submission #469830.

15

## 16 **TUBE pulldown**

17 Endogenous poly-Ub conjugates were purified from cells using TUBE affinity reagents  
18 (LifeSensors, UM401). Cells were lysed in buffer containing 50 mM Tris-HCl pH 7.5,  
19 0.15 M NaCl, 1mM EDTA, 1% NP-40, 10% glycerol supplemented with complete  
20 protease inhibitor cocktail, PR-619 and 1,10-phenanthroline. Lysate was cleared by  
21 centrifugation, Agarose-TUBEs were added, and pulldown was performed for 16 h at  
22 4 °C on rotation. The beads were then washed three times with 1 ml of ice-cold TBS-  
23 T, and bound material was eluted by mixing the beads with sample buffer and heating  
24 to 95 °C for 5 min.

25



## 1 **Statistical analysis**

2 Data are represented as mean  $\pm$  S.E.M.. Statistical significance was calculated with  
3 the unpaired two-tailed Student's t test, one-way or two-way analysis of variance  
4 (ANOVA) followed by multiple comparison test using GraphPad Prism software. A *P*  
5 value that was less than 0.05 was considered to be statistically significant for all data  
6 sets. Significant differences between experimental groups were: \**p* < 0.05, \*\**p* < 0.01  
7 or \*\*\* *p* < 0.001. Biological replicates represent experiments performed on samples  
8 from separate biological preparations; technical replicates represent samples from the  
9 same biological preparation run in parallel.

## 1 **Acknowledgements**

2 Part of this work was funded by Forma Therapeutics. This work was also supported  
3 by the Francis Crick Institute which receives its core funding from Cancer Research  
4 UK (FC001039), the UK Medical Research Council (FC001039), and the Wellcome  
5 Trust (FC001039). We thank the Discovery Proteomics Facility (led by Dr Roman  
6 Fischer) at the Target Discovery Institute (Oxford) for expert help with the analysis by  
7 mass spectrometry. Work in the B.M.K. laboratory was supported by a John Fell  
8 Fund 133/075, the Wellcome Trust (097813/Z/11/Z) and the Engineering and  
9 Physical Sciences Research Council (EP/N034295/1).

10

## 11 **Author Contributions**

12 EJR, CJD, TRH, SK, DK, NJ, MW, SU, MJC, BMK and AB designed the study. EJR,  
13 LL, EMR, CDC, IR, NM and EN performed mouse genetics and in vivo experiments.  
14 EJR, TMC, AD, GV, HCS, CH and APF performed biochemical experiments with the  
15 help of APT, WWK, MG, DK and BMK. DG, JK, MK, CM, SI, JCC and CJD designed  
16 and characterised small molecule inhibitors. All authors commented on the  
17 manuscript. EJR, APF, BMK and AB wrote the manuscript.

18

## 19 **Declaration of Interests**

20 None of the authors from pharmaceutical companies declare competing financial  
21 interests with their current affiliations. The authors APT, WWK, DG, JK, SI, MK, CK,  
22 JOC, NJ, CH, TRH, DK, SK, SU, MJC, BMK and AB declare competing financial  
23 interests due to financial support for the project described in this manuscript by Forma  
24 Therapeutics, Watertown, MA, USA.

25

1 **Figure legends**

2 **Figure 1. MYC, JUN and  $\Delta p63$  are highly expressed in LSCC tumors**

3 A) Expression of *MYC* in human lung adenocarcinoma (LADC, n = 483), lung  
4 squamous cell carcinoma (LSCC, n = 486), and normal non-transformed tissue  
5 (normal LSCC = 338, normal LADC = 347). In box plots, the centre line reflects the  
6 median. Data from TCGA and GTEx were analyzed using GEPIA software.

7 B) Relative mRNA expression of *MYC* in normal lung tissue (n = 5) and LSCC (n = 17)  
8 patient samples from the Cordoba Biobank measured by RT-PCR. The P value was  
9 calculated using the Student's two-tailed t test. Plots indicate mean.

10 C) Representative LADC and LSCC tumors stained with c-Myc, c-Jun and  $\Delta p63$   
11 antibodies. Scale bars, 30  $\mu$ m.

12 D) Quantification of c-Myc<sup>+</sup> (LADC n = 33, LSCC n = 34), c-Jun<sup>+</sup> (LADC n = 33, LSCC  
13 n = 33) and  $\Delta p63$ <sup>+</sup> cells (LADC n = 41, LSCC n = 41) in LADC and LSCC tumors.  
14 Plots indicate mean. Student's two-tailed t test was used to calculate P values.

15 E) Graph showing the difference in cell proliferation between control and MYC-  
16 depleted KF LSCC cells (n = 3). Graph indicates mean  $\pm$  S.E.M.. Student's two-tailed  
17 t test was used to calculate P values.

18 F) Genetic alterations in *USP28* and *FBXW7* genes in human LSCC. Each column  
19 represents a tumor sample (n = 178). Data from TCGA were analyzed using cBioportal  
20 software.

21 G) Relative mRNA expression of *USP28* in normal lung tissue (n = 5) and LSCC (n =  
22 17) patient samples from the Cordoba Biobank measured by RT-PCR. The P value  
23 was calculated using the Student's two-tailed t test. Plots indicate mean. See also  
24 Supplementary Figure S2B.

1 H) shRNA-mediated knockdown of Usp28 decreases c-Myc, c-Jun and  $\Delta$ p63 protein  
2 levels in primary KF LSCC cells.

3 I) Graph showing the difference in cell proliferation between control and Usp28-  
4 depleted KF LSCC cells (n = 3). Graph indicates mean  $\pm$  S.E.M.. One-way ANOVA  
5 with Dunnett's multiple comparisons test was used to calculate P values.

6

## 7 **Figure 2. Usp28 is an effective therapeutic target for LSCC tumors**

8 A) Schematic representation of the KFCU (FSF-Kras<sup>G12D</sup>; Ebxw7<sup>FRT/FRT</sup>; ROSA26-  
9 FSF-Cre<sup>ERT</sup>; Usp28<sup>flox/flox</sup>) model and experimental approach used to deplete  
10 conditional Usp28 alleles in established lung tumors.

11 B) Lung histology of animals treated as in A, showing both LSCC (CK5<sup>+</sup>) and LADC  
12 (Sftpc<sup>+</sup>) tumors in mice receiving vehicle but few LSCC lesions in mice receiving  
13 tamoxifen. Scale bars, 1000  $\mu$ m.

14 C) Quantification of LADC tumors in vehicle-, tamoxifen- and tamoxifen+FT206 treated  
15 KFCU mice. Plots indicate mean. One-way ANOVA with Tukey's multiple  
16 'comparisons test was used to calculate P values (n = 8 vehicle, n = 7 tamoxifen, n =  
17 7 tamoxifen + FT206).

18 D) Quantification of LADC tumor size in vehicle-, tamoxifen- and tamoxifen+FT206  
19 treated KFCU mice. Plots indicate mean. One-way ANOVA with Tukey's multiple  
20 'comparisons test was used to calculate P values (n = 466 vehicle, n = 434 tamoxifen,  
21 n = 503 tamoxifen + FT206).

22 E) Immunoblot analysis of LADC tumors probed for Usp28, c-Myc, c-Jun, Sftpc,  
23 cleaved caspase-3 (CC3). Vinculin is shown as loading control.

24 F) Quantification of LSCC tumors in vehicle-, tamoxifen- and tamoxifen+FT206 treated  
25 KFCU mice. Plots indicate mean. One-way ANOVA with Tukey's multiple

1 'comparisons test was used to calculate P values (n = 8 vehicle, n = 7 tamoxifen, n =  
2 7 tamoxifen + FT206).

3 G) Quantification of LSCC tumor size in vehicle-, tamoxifen- and tamoxifen+FT206  
4 treated KFCU mice. Plots indicate mean. One-way ANOVA with Tukey's multiple  
5 'comparisons test was used to calculate P values (n = 326 vehicle, n = 103 tamoxifen,  
6 n = 79 tamoxifen + FT206).

7 H) *Usp28* deletion induces apoptotic cell death (cleaved caspase-3, CC3) and  
8 decreases c-Myc, c-Jun and  $\Delta$ p63 protein levels in LSCC lesions.

9

10 **Figure 3. *Usp28* is not a therapeutic target for advanced KRas<sup>G12D</sup>; Trp53 mutant**  
11 **tumors**

12 A) Schematic representation of the KPCU (FSF-KRas<sup>G12D</sup>; p53<sup>FRT/FRT</sup>; ROSA26-FSF-  
13 Cre<sup>ERT</sup>; Usp28<sup>flox/flox</sup>; ROSA26-LSL-mTmG) model and experimental approach used.  
14 At 10-weeks post-infection, KPCU mice were treated with vehicle or tamoxifen.

15 B) Representative images of H&E (left) and GFP (right) stains from mice of the  
16 indicated treatments. Scale bar, 1000  $\mu$ m.

17 C) Quantification of mouse LADC tumors in the KPCU model. Plots indicate mean.  
18 Student's two-tailed t test was used to calculate P values (n = 10 vehicle, n = 10  
19 tamoxifen).

20 D) Quantification of LADC tumor size in vehicle- and tamoxifen-treated KPCU mice.  
21 Plots indicate mean. Student's two-tailed t test was used to calculate P values (n =  
22 110 vehicle, n = 130 tamoxifen).

23 E) Representative images illustrating histological analysis of lung lesions in KPCU  
24 mice, treated with vehicle or tamoxifen. H&E, Sftpc, TTF1, GFP immunohistochemistry

1 staining and in situ hybridization of USP28 and PPIB mRNA expression. Scale bars,  
2 50  $\mu$ m.

3

#### 4 **Figure 4. USP28 inhibitor selectivity and cellular target engagement**

5 A) Structure of small molecular inhibitor FT3951206/CRT0511973 (FT206).

6 B) Cellular DUB profiling in NCI-H520 LSCC cell extracts incubated with the indicated  
7 concentrations of FT206 prior to labelling with HA-UbPA, SDS-PAGE and analysis by  
8 Western blotting. Inhibitor potency was reflected by competition with USP28/25-ABP  
9 adduct formation.

10 C) Cellular DUB profiling in NCI-H520 LSCC cells incubated with the indicated  
11 concentrations of FT206, lysed extracts labelled with HA-UbPA and analysed as in B.

12 D) Activity-based Probe Profiling (ABPP) demonstrating the cellular DUB selectivity  
13 profile of cpd FT206 by quantitative mass spectrometry analysis at different inhibitor  
14 concentrations. Graph indicates mean  $\pm$  S.E.M..

15 E) Usp28 inhibition using FT206 (50nM and 100nM) reduces c-Myc, c-Jun and  $\Delta$ p63  
16 protein levels in primary KF LSCC cells.

17 F) Usp28 inhibition using FT206 decreases cell proliferation in KF LSCC cells (n = 4).  
18 Graph indicates mean  $\pm$  S.E.M..

19

#### 20 **Figure 5. Pharmacologic USP28 inhibition reduces c-Myc, c-Jun and $\Delta$ p63** 21 **protein levels in mouse LSCC tumors, and induces tumor cell death**

22 A) Scheme depicting experimental design for in vivo test of FT206 (75mg/kg), 3 times  
23 a week for 5 weeks.

- 1 B) Lung histology of animals treated as in A, showing both LSCC (CK5<sup>+</sup>) and LADC  
2 (Sftpc<sup>+</sup>) tumors in LSL-KRas<sup>G12D</sup>; Fbxw7<sup>ff</sup> (KF) mice receiving vehicle but few LSCC  
3 lesions in mice receiving FT206. Scale bars, 1000  $\mu$ m.
- 4 C) Quantification of LADC tumors per animal in vehicle- and FT206-treated KF mice.  
5 Plots indicate mean. P values calculated using Student's two-tailed t test (n = 7 vehicle,  
6 n = 10 FT206).
- 7 D) Quantification of LADC tumor size in vehicle- and FT206-treated KF mice. Plots  
8 indicate mean. Student's two-tailed t test was used to calculate P values (n = 304  
9 vehicle, n = 481 FT206).
- 10 E) Quantification of LSCC tumors per animal in vehicle- and FT206-treated KF mice.  
11 Plots indicate mean. P values calculated using Student's two-tailed t test (n = 7 vehicle,  
12 n = 10 FT206).
- 13 F) Quantification of LSCC tumor size in vehicle- and FT206-treated KF mice. Plots  
14 indicate mean. Student's two-tailed t test was used to calculate P values (n = 156  
15 vehicle, n = 96 FT206).
- 16 G) LSCC tumors stained with c-Myc, c-Jun and  $\Delta$ p63 antibodies. KF animals treated  
17 with vehicle (left panel) or FT206 (right panel). Inserts showing c-Myc<sup>+</sup>, c-Jun<sup>+</sup>,  $\Delta$ p63<sup>+</sup>  
18 LSCC tumors in mice receiving vehicle (left panel) but partial positive or negative  
19 LSCC lesions in mice receiving FT206 (right panel). Scale bars, 50  $\mu$ m.
- 20 H) Scheme depicting experimental design for in vivo test of FT206 (75 mg/kg) for 4  
21 days consecutively (upper panel). Cleaved caspase-3 (CC3) stain shows apoptotic  
22 cells (bottom panel). Scale bars, 50  $\mu$ m.
- 23 I) Quantification of cleaved caspase-3 (CC3)-positive cells per field (20x) in LADC (n  
24 = 114 vehicle, 203 FT206) and LSCC (n = 94 vehicle, 167 FT206) tumors from KF

1 mice treated as in H. Plots indicate mean. Student's two-tailed t test was used to  
2 calculate P values.

3 See also Supplementary Figure S5.

4

5 **Figure 6. Pharmacological inhibition of USP28 prevents human LSCC tumor**  
6 **progression and reduces c-Myc protein levels in xenograft models**

7 A) siRNA-mediated knockdown of USP28 decreases c-Myc, c-Jun and  $\Delta$ p63 protein  
8 levels in human LUDLU-1 LSCC cells.

9 B) USP28 inhibition using FT206 (0.2 and 0.4  $\mu$ M) reduces c-Myc, c-Jun and  $\Delta$ p63  
10 protein levels in human LUDLU-1 LSCC cells.

11 C) USP28 inhibition using FT206 decreases cell proliferation in human LSCC (NCI-  
12 H520, CALU-1 and LUDLU-1) cell lines (n = 8). Graphs indicate mean  $\pm$  S.E.M..

13 D, E, F) In vivo tumor graft growth curves of human LSCC (NCI-H520, CALU-1 and  
14 LUDLU-1) cell lines subcutaneously injected in flanks of immunocompromised mice.

15 Animals with palpable tumors were treated with vehicle or FT206 (75mg/kg) via oral  
16 gavage. Plots indicate mean  $\pm$  SD of the tumor volumes. P values calculated from two-  
17 way ANOVA with Bonferroni's multiple comparisons test (NCI-H520 n = 4 vehicle and  
18 4 FT206; CALU-1 n = 3 vehicle and 3 FT206; LUDLU-1 n = 3 vehicle and 3 FT206).

19 G, H, I) Mice treated as in D, E and F, respectively. Plots showing the weight of  
20 xenograft tumors at the end point. Student's two-tailed t test was used to calculate P  
21 values (NCI-H520 n = 4 vehicle and 4 FT206; CALU-1 n = 3 vehicle and 3 FT206;  
22 LUDLU-1 n = 3 vehicle and 3 FT206).

23 J, K, L) c-Myc immunohistochemistry stainings of NCI-H520, CALU-1 and LUDLU-1  
24 xenografts in mice treated as in D, E and F, respectively. Scale bars, 50  $\mu$ m.

25



1 **Supplementary figure legends**

2 **Supplementary Figure S1, related to Figure 1.**

3 A) Graphs showing the difference in cell proliferation between control and siMYC-  
4 transfected human LSCC cell lines (NCI-H226, NCI-H520, CALU-1 and LUDLU-1).  
5 Graphs indicate mean  $\pm$  S.E.M.. P values calculated using one-way ANOVA with  
6 Tukey's multiple comparisons test.

7 B) Graphs showing the difference in cell proliferation between control and siJUN-  
8 transfected human LSCC cell lines (NCI-H226, NCI-H520, CALU-1 and LUDLU-1).  
9 Graphs indicate mean  $\pm$  S.E.M.. P values calculated using one-way ANOVA with  
10 Tukey's multiple comparisons test.

11 C) Graphs showing the difference in cell proliferation between control and si $\Delta$ Np63-  
12 transfected human LSCC cell lines (NCI-H226, NCI-H520, CALU-1 and LUDLU-1).  
13 Graphs indicate mean  $\pm$  S.E.M.. P values calculated using one-way ANOVA with  
14 Tukey's multiple comparisons test.

15

16 **Supplementary Figure S2, related to Figure 1.**

17 A) Dot plot showing association between the log<sub>2</sub> mRNA expression (Y-axis) and copy-  
18 number alterations (X-axis) for USP28 gene. Data from TCGA were analyzed using  
19 cBioportal software. One-way ANOVA with Bonferroni's multiple comparisons test was  
20 used to calculate P values (n = 2 Deep deletion, n = 57 Shallow deletion, n = 81 Diploid,  
21 n = 38 Gain).

22 B) Representative human LSCC tumors stained with USP28 and FBW7 antibodies.  
23 Scale bars, 100  $\mu$ m (left panel). Quantification of USP28 and FBW7 protein staining  
24 in LSCC tumors (n = 17) (right panel).

25

1 **Supplementary Figure S3, related to Figure 2. Gene targeting strategy to**  
2 **generate a Fbxw7 FRT/FRT allele that can be deleted by Flp recombinase.**

3 A) Gene targeting strategy to generate conditional Fbxw7<sup>FRT/FRT</sup> animals. Two FRT  
4 sites were inserted into the intron 4 and 5 of Fbxw7 through the CRISPR-Cas9  
5 technology.

6 B) Schematic representation of the conditional allele (left panel). In vitro recombination  
7 assay demonstrated efficient ablation of the exon 5 upon Flp recombinase adenovirus  
8 infection (right panel).

9 C) KFCU (FSF-KRas<sup>G12D</sup>; Fbxw7<sup>FRT/FRT</sup>; ROSA26-FSF-Cre<sup>ERT</sup>; Usp28<sup>flox/flox</sup>) mice  
10 infected with adeno-CMV-Flp virus develop LADC (Sftpc<sup>+</sup> and TTF1<sup>+</sup>) and LSCC  
11 (CK5<sup>+</sup> and Δp63<sup>+</sup>) tumors.

12 D) In situ hybridization of *USP28* and *PPIB* mRNA expression in vehicle- and  
13 tamoxifen-treated KFCU mice. Scale bars, 50 μm.

14 E) KFCU tumors stained with c-Myc, c-Jun and Δp63 antibodies. KFCU mice treated  
15 with vehicle (left panel) or tamoxifen (right panel). Inserts showing c-Myc<sup>+</sup>, c-Jun<sup>+</sup> and  
16 Δp63<sup>+</sup> LSCC tumors in mice receiving vehicle but partial positive or negative LSCC  
17 lesions in mice receiving tamoxifen. Scale bars, 50 μm.

18

19 **Supplementary Figure S4, related to Figure 4.**

20 A) Comparison of USP28/25 inhibitor potency by activity-based profiling. Human  
21 LSCC H520 crude cell extracts were incubated either with AZ1 or FT206 inhibitors at  
22 indicated concentrations, followed by HA-UbPA activity-based probe (ABP) labelling.  
23 Samples were analysed by SDS-PAGE and immunoblotted using USP28, USP25, HA,  
24 and GAPDH antibodies. Inhibitor potency was reflected by competition with  
25 USP28/25-ABP adduct formation.

1 B) TUBE pulldown of endogenous ubiquitylated c-Myc, c-Jun and USP28 in LSCC  
2 cells upon co-treatment with MG132 and FT206.

3 C) Immunoblot of endogenous USP28, c-Jun, c-Myc and  $\Delta p63$  in LSCC cells upon co-  
4 treatment with MG132 and FT206. Vinculin served as loading control.

5 D) Graphs showing the difference in cell proliferation between control, FT206-treated  
6 and USP28-depleted LSCC cells. Graph indicates mean  $\pm$  S.E.M.. One-way ANOVA  
7 with Tukey's multiple comparisons test was used to calculate P values. Vinculin is  
8 shown as loading control.

9

10 **Supplementary Figure S5, related to Figure 5.**

11 A) Monitoring tolerability in mice treated with FT206 (75mg/kg), 3 times a week for 5  
12 weeks. Body weights of animals during the course of treatment (n = 3 vehicle, n = 3  
13 FT206).

14 B) Kidney, liver and spleen sections stained with H&E. Mice treated as in A. Bars, 100  
15  $\mu\text{m}$ .

16

17 **Supplementary Figure S6, related to Figure 6.**

18 A) Immunoblot of endogenous c-Myc and c-Jun in LSCC cells upon FT206 treatment  
19 (IC50 doses display in panel C). Vinculin served as loading control.

20 B) Immunoblot of endogenous c-Myc and c-Jun in LADC cells upon FT206 treatment  
21 (IC50 doses display in panel C). Vinculin served as loading control.

22 C) IC50 values (doses that inhibits 50% of the cell viability) were calculated after  
23 exposure of human LADC and LSCC cells to different concentrations of FT206  
24 compound.

## 1   **References**

2

3   Altun, M., Kramer, H. B., Willems, L. I., McDermott, J. L., Leach, C. A., Goldenberg, S. J., Kumar,  
4       K. G., Konietzny, R., Fischer, R., Kogan, E., *et al.* (2011). Activity-based chemical proteomics  
5       accelerates inhibitor development for deubiquitylating enzymes. *Chem Biol* *18*, 1401-  
6       1412.

7   Benns, H. J., Wincott, C. J., Tate, E. W., and Child, M. A. (2021). Activity- and reactivity-based  
8       proteomics: Recent technological advances and applications in drug discovery. *Curr Opin*  
9       *Chem Biol* *60*, 20-29.

10   Cancer Genome Atlas Research, N. (2012). Comprehensive genomic characterization of  
11       squamous cell lung cancers. *Nature* *489*, 519-525.

12   Cardarella, S., and Johnson, B. E. (2013). The impact of genomic changes on treatment of lung  
13       cancer. *Am J Respir Crit Care Med* *188*, 770-775.

14   Cerami, E., Gao, J., Dogrusoz, U., Gross, B. E., Sumer, S. O., Aksoy, B. A., Jacobsen, A., Byrne,  
15       C. J., Heuer, M. L., Larsson, E., *et al.* (2012). The cBio cancer genomics portal: an open  
16       platform for exploring multidimensional cancer genomics data. *Cancer Discov* *2*, 401-404.

17   Clancy, A., Heride, C., Pinto-Fernandez, A., Elcocks, H., Kallinos, A., Kayser-Bricker, K. J., Wang,  
18       W., Smith, V., Davis, S., Fessler, S., *et al.* (2021). Correction: The deubiquitylase USP9X  
19       controls ribosomal stalling. *J Cell Biol* *220*.

20   Davis, R. J., Welcker, M., and Clurman, B. E. (2014). Tumor suppression by the Fbw7 ubiquitin  
21       ligase: mechanisms and opportunities. *Cancer Cell* *26*, 455-464.

22   de Bie, P., and Ciechanover, A. (2011). Ubiquitination of E3 ligases: self-regulation of the  
23       ubiquitin system via proteolytic and non-proteolytic mechanisms. *Cell Death Differ* *18*,  
24       1393-1402.

25   Diefenbacher, M. E., Chakraborty, A., Blake, S. M., Mitter, R., Popov, N., Eilers, M., and  
26       Behrens, A. (2015). Usp28 counteracts Fbw7 in intestinal homeostasis and cancer. *Cancer*  
27       *Res* *75*, 1181-1186.

28   Diefenbacher, M. E., Popov, N., Blake, S. M., Schulein-Volk, C., Nye, E., Spencer-Dene, B.,  
29       Jaenicke, L. A., Eilers, M., and Behrens, A. (2014). The deubiquitinase USP28 controls  
30       intestinal homeostasis and promotes colorectal cancer. *The Journal of clinical investigation*  
31       *124*, 3407-3418.

32   Fennell, D. A., Summers, Y., Cadranel, J., Benepal, T., Christoph, D. C., Lal, R., Das, M., Maxwell,  
33       F., Visseren-Grul, C., and Ferry, D. (2016). Cisplatin in the modern era: The backbone of  
34       first-line chemotherapy for non-small cell lung cancer. *Cancer Treat Rev* *44*, 42-50.

35   Gandara, D. R., Hammerman, P. S., Sos, M. L., Lara, P. N., Jr., and Hirsch, F. R. (2015).  
36       Squamous cell lung cancer: from tumor genomics to cancer therapeutics. *Clin Cancer Res*  
37       *21*, 2236-2243.

38   Guerin, D., Bair, K., Caravella, J.A., Ioannidis, S., Lancia, D.R., Li, H., Mischke, S., Ng, P.Y.,  
39       Richard, D., Schiller, S., et al. (2017). THIENOPYRIDINE CARBOXAMIDES AS UBIQUITIN-  
40       SPECIFIC PROTEASE INHIBITORS In USA: World Intellectual Property Organization  
41       International Bureau, (USA).

42   Guerin, D., Ng, P. Y., Wang, Z., Shelekhin, T., Caravella, J., Zablocki, M.-M., Downing, J. R., Li,  
43       H., and Ioannidis, S. (2020). CARBOXAMIDES AS UBIQUITIN-SPECIFIC PROTEASE  
44       INHIBITORS In: World Intellectual Property Organization International Bureau. In World  
45       Intellectual Property Organization International Bureau.

- 1 Hirsch, F. R., Govindan, R., Zvirbule, Z., Braiteh, F., Rittmeyer, A., Belda-Iniesta, C., Isla, D.,  
2 Cosgriff, T., Boyer, M., Ueda, M., *et al.* (2017). Efficacy and Safety Results From a Phase II,  
3 Placebo-Controlled Study of Onartuzumab Plus First-Line Platinum-Doublet Chemotherapy  
4 for Advanced Squamous Cell Non-Small-Cell Lung Cancer. *Clin Lung Cancer* *18*, 43-49.
- 5 Isaka, T., Nakayama, H., Yokose, T., Ito, H., Katayama, K., Yamada, K., and Masuda, M. (2017).  
6 Platinum-Based Adjuvant Chemotherapy for Stage II and Stage III Squamous Cell  
7 Carcinoma of the Lung. *Ann Thorac Cardiovasc Surg* *23*, 19-25.
- 8 Jackson, E. L., Willis, N., Mercer, K., Bronson, R. T., Crowley, D., Montoya, R., Jacks, T., and  
9 Tuveson, D. A. (2001). Analysis of lung tumor initiation and progression using conditional  
10 expression of oncogenic K-ras. *Genes & development* *15*, 3243-3248.
- 11 Jandke, A., Da Costa, C., Sancho, R., Nye, E., Spencer-Dene, B., and Behrens, A. (2011). The F-  
12 box protein Fbw7 is required for cerebellar development. *Dev Biol* *358*, 201-212.
- 13 Jones, H. B. L., Heilig, R., Fischer, R., Kessler, B. M., and Pinto-Fernandez, A. (2021). ABPP-HT  
14 - High-Throughput Activity-Based Profiling of Deubiquitylating Enzyme Inhibitors in a  
15 Cellular Context. *Front Chem* *9*, 640105.
- 16 Kan, Z., Jaiswal, B. S., Stinson, J., Janakiraman, V., Bhatt, D., Stern, H. M., Yue, P., Haverty, P.  
17 M., Bourgon, R., Zheng, J., *et al.* (2010). Diverse somatic mutation patterns and pathway  
18 alterations in human cancers. *Nature* *466*, 869-873.
- 19 Knobel, P. A., Belotserkovskaya, R., Galanty, Y., Schmidt, C. K., Jackson, S. P., and Stracker, T.  
20 H. (2014). USP28 Is Recruited to Sites of DNA Damage by the Tandem BRCT Domains of  
21 53BP1 but Plays a Minor Role in Double-Strand Break Metabolism. *Molecular and cellular  
22 biology* *34*, 2062-2074.
- 23 Liao, R. G., Watanabe, H., Meyerson, M., and Hammerman, P. S. (2012). Targeted therapy for  
24 squamous cell lung cancer. *Lung Cancer Manag* *1*, 293-300.
- 25 Muzumdar, M. D., Tasic, B., Miyamichi, K., Li, L., and Luo, L. (2007). A global double-  
26 fluorescent Cre reporter mouse. *Genesis* *45*, 593-605.
- 27 Novello, S., Scagliotti, G. V., Sydorenko, O., Vynnychenko, I., Volovat, C., Schneider, C. P.,  
28 Blackhall, F., McCoy, S., Hei, Y. J., and Spigel, D. R. (2014). Motesanib plus  
29 carboplatin/paclitaxel in patients with advanced squamous non-small-cell lung cancer:  
30 results from the randomized controlled MONET1 study. *J Thorac Oncol* *9*, 1154-1161.
- 31 Panyain, N., Godinat, A., Lanyon-Hogg, T., Lachiondo-Ortega, S., Will, E. J., Soudy, C., Mondal,  
32 M., Mason, K., Elkhalfi, S., Smith, L. M., *et al.* (2020). Discovery of a Potent and Selective  
33 Covalent Inhibitor and Activity-Based Probe for the Deubiquitylating Enzyme UCHL1, with  
34 Antifibrotic Activity. *J Am Chem Soc* *142*, 12020-12026.
- 35 Pinto-Fernandez, A., Davis, S., Schofield, A. B., Scott, H. C., Zhang, P., Salah, E., Mathea, S.,  
36 Charles, P. D., Damianou, A., Bond, G., *et al.* (2019). Comprehensive Landscape of Active  
37 Deubiquitinating Enzymes Profiled by Advanced Chemoproteomics. *Front Chem* *7*, 592.
- 38 Popov, N., Wanzel, M., Madiredjo, M., Zhang, D., Beijersbergen, R., Bernards, R., Moll, R.,  
39 Elledge, S. J., and Eilers, M. (2007). The ubiquitin-specific protease USP28 is required for  
40 MYC stability. *Nat Cell Biol* *9*, 765-774.
- 41 Prieto-Garcia, C., Hartmann, O., Reissland, M., Braun, F., Fischer, T., Walz, S., Schulein-Volk,  
42 C., Eilers, U., Ade, C. P., Calzado, M. A., *et al.* (2020). Maintaining protein stability of Np63  
43 via USP28 is required by squamous cancer cells. *EMBO Mol Med* *12*, e11101.
- 44 Ruiz, E. J., Diefenbacher, M. E., Nelson, J. K., Sancho, R., Pucci, F., Chakraborty, A., Moreno,  
45 P., Annibaldi, A., Llicardi, G., Encheva, V., *et al.* (2019). LUBAC determines chemotherapy  
46 resistance in squamous cell lung cancer. *J Exp Med* *216*, 450-465.

- 1 Scagliotti, G. V., Parikh, P., von Pawel, J., Biesma, B., Vansteenkiste, J., Manegold, C.,  
2 Serwatowski, P., Gatzemeier, U., Digumarti, R., Zukin, M., *et al.* (2008). Phase III study  
3 comparing cisplatin plus gemcitabine with cisplatin plus pemetrexed in chemotherapy-  
4 naive patients with advanced-stage non-small-cell lung cancer. *J Clin Oncol* *26*, 3543-3551.
- 5 Schauer, N. J., Magin, R. S., Liu, X., Doherty, L. M., and Buhrlage, S. J. (2019). Advances in  
6 Discovering Deubiquitinating Enzyme (DUB) Inhibitors. *J Med Chem*.
- 7 Schonhuber, N., Seidler, B., Schuck, K., Veltkamp, C., Schachtler, C., Zukowska, M., Eser, S.,  
8 Feyerabend, T. B., Paul, M. C., Eser, P., *et al.* (2014). A next-generation dual-recombinase  
9 system for time- and host-specific targeting of pancreatic cancer. *Nature medicine* *20*,  
10 1340-1347.
- 11 Turnbull, A. P., Ioannidis, S., Krajewski, W. W., Pinto-Fernandez, A., Heride, C., Martin, A. C.  
12 L., Tonkin, L. M., Townsend, E. C., Buker, S. M., Lancia, D. R., *et al.* (2017). Molecular basis  
13 of USP7 inhibition by selective small-molecule inhibitors. *Nature* *550*, 481-486.
- 14 Wrigley, J. D., Gavory, G., Simpson, I., Preston, M., Plant, H., Bradley, J., Goepfert, A. U.,  
15 Rozycka, E., Davies, G., Walsh, J., *et al.* (2017). Identification and Characterization of Dual  
16 Inhibitors of the USP25/28 Deubiquitinating Enzyme Subfamily. *ACS Chem Biol* *12*, 3113-  
17 3125.
- 18 Zablocki, M.-M., Guerin, D., Ng, P. Y., Wang, Z., Shelekhin, T., Caravella, J., Li, H., and Ioannidis,  
19 S. (2019). CARBOXAMIDES AS UBIQUITIN-SPECIFIC PROTEASE INHIBITORS In: World  
20 Intellectual Property Organization International Bureau, (France). In USA: World  
21 Intellectual Property Organization International Bureau, (USA).

22  
23

1 **Table 1: Primers for qPCR**

Name	Primer (5'–3')	
	Forward	Reverse
ACTIN	GAAAATCTGGCACCACACCT	TAGCACAGCCTGGATAGCAA
USP28	ACTCAGACTATTGAACAGATGTACTGC	CTGCATGCAAGCGATAAGG
MYC	TCTCCTTGCAGCTGCTTAG	GTCGTAGTCGAGGTCATAG

2

3 **Table 2: List of Reagents**

REAGENT	SOURCE	IDENTIFIER
<b>Antibodies</b>		
Rabbit anti-CK5	Abcam	ab52635
Rabbit anti-c-Myc	Abcam	ab32072
Goat anti-GFP	Abcam	ab6673
Rabbit anti-Ki67	Abcam	ab16667
Rabbit anti-TTF1	Abcam	ab76013
Rabbit anti-USP28	Abcam	ab126604
Rabbit anti-USP25	Abcam	ab187156
Rabbit anti-USP11	Abcam	ab109232
Rabbit anti-USP36	Abcam	ab102565
Rabbit anti-actin	Abcam	ab8227
Rabbit anti-USP28	Atlas	HPA006779
Rabbit anti- $\Delta$ p63	Biologend	619001
Mouse anti-c-Jun	BD Biosciences	610326
Rabbit anti-FBW7	Bethyl	A301-721A
Rabbit anti-USP7	Enzo	BML-PW0540
Mouse anti-GAPDH	Invitrogen	MA5-15738
Rabbit anti-Sftpc	Millipore	ab3786
Rabbit anti-caspase 3 active	R&D Systems	AF835
Rat anti-HA	Roche	11666606001
Mouse anti-tubulin	Sigma	T5168
<b>Virus Strains</b>		
Adeno-CMV-Cre	UI viral vector core	VVC-U of Iowa-5-HT
Adeno-CMV-Flp	UI viral vector core	VVC-U of Iowa-530HT
<b>Chemicals, Peptides, and Recombinant Proteins</b>		
Doxycycline hyclate	Sigma	D9891
Tamoxifen	Sigma	T5648

4

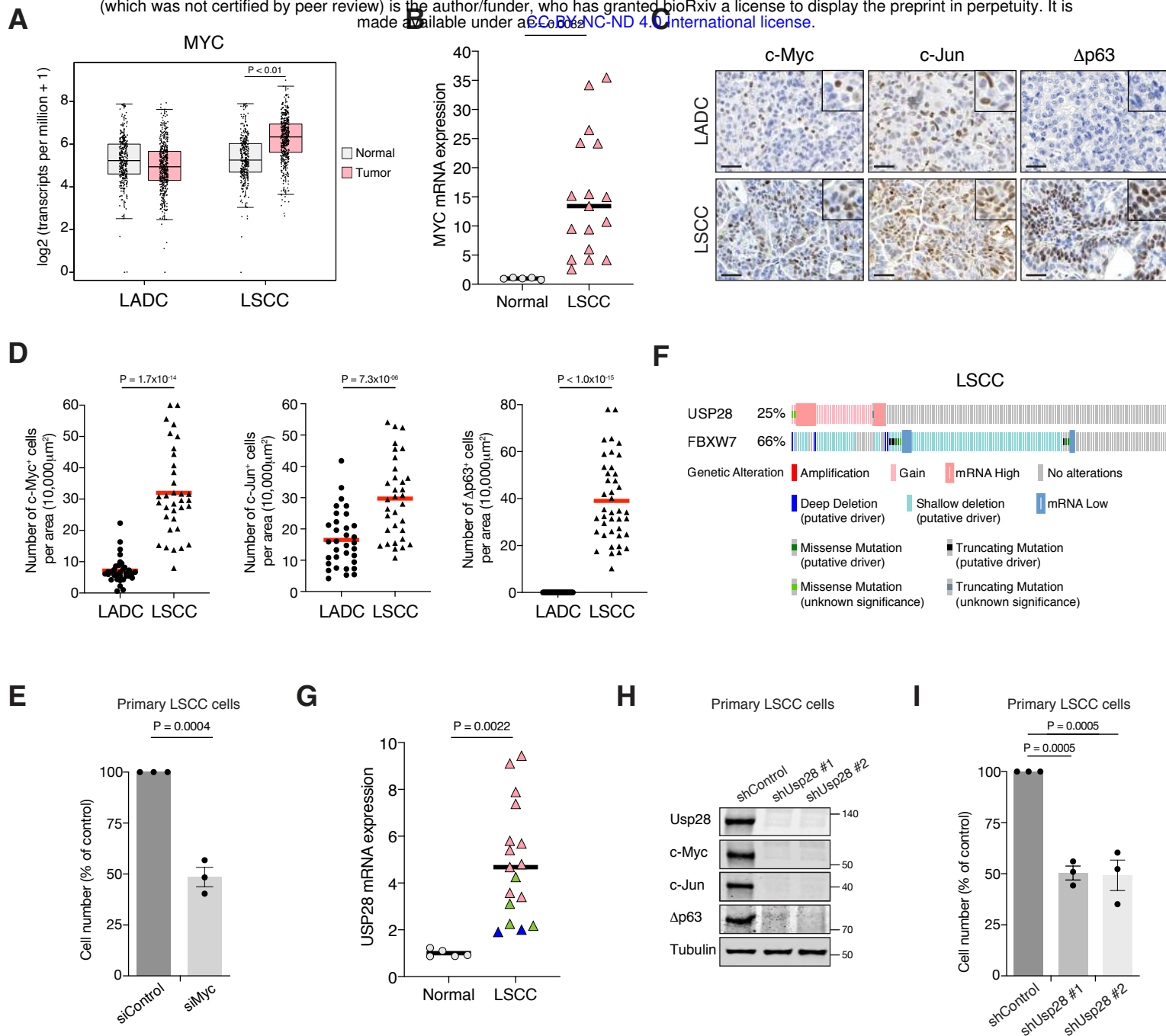
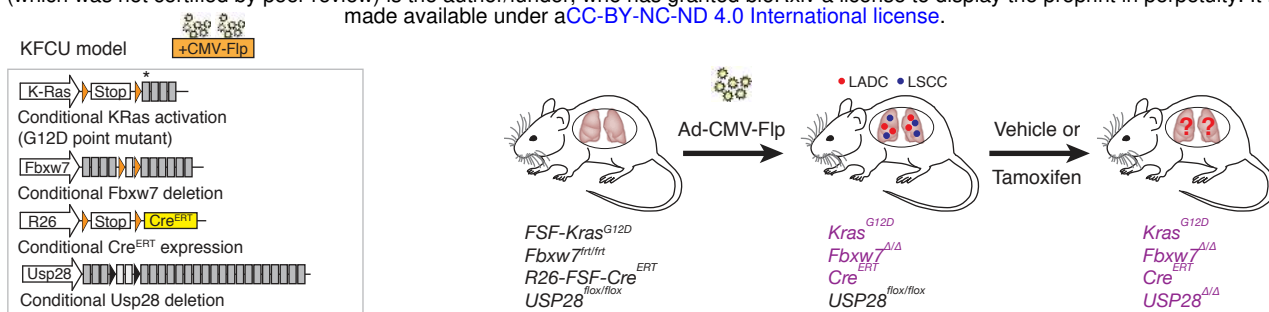


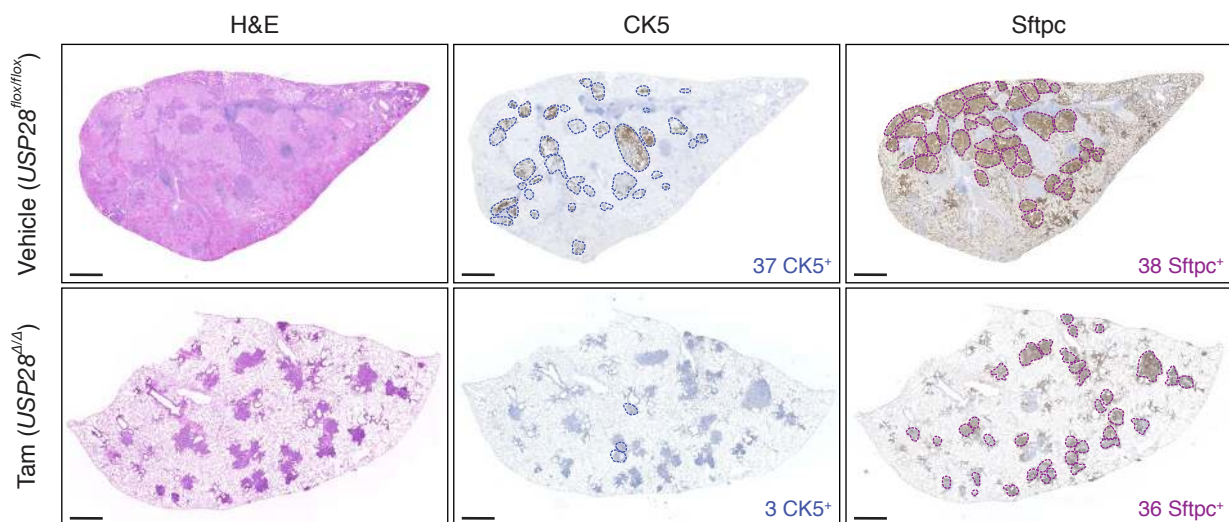
**Figure 1**



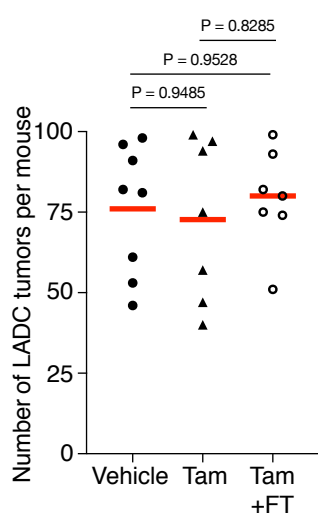
**A**



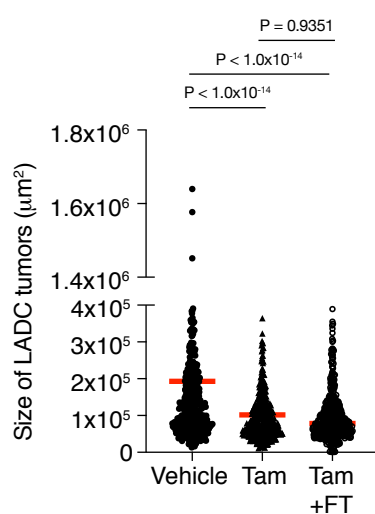
**B**



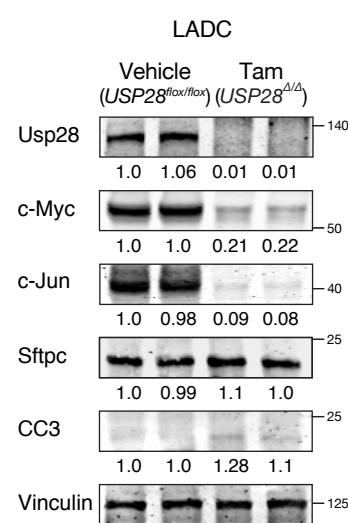
**C**



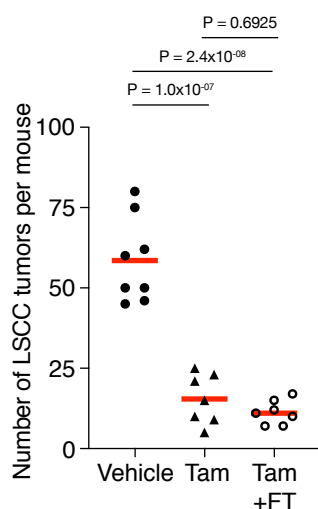
**D**



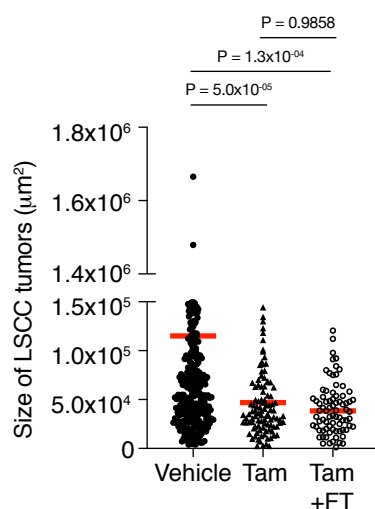
**E**



**F**



**G**



**H**

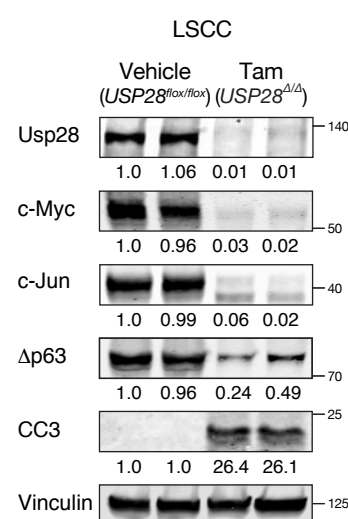
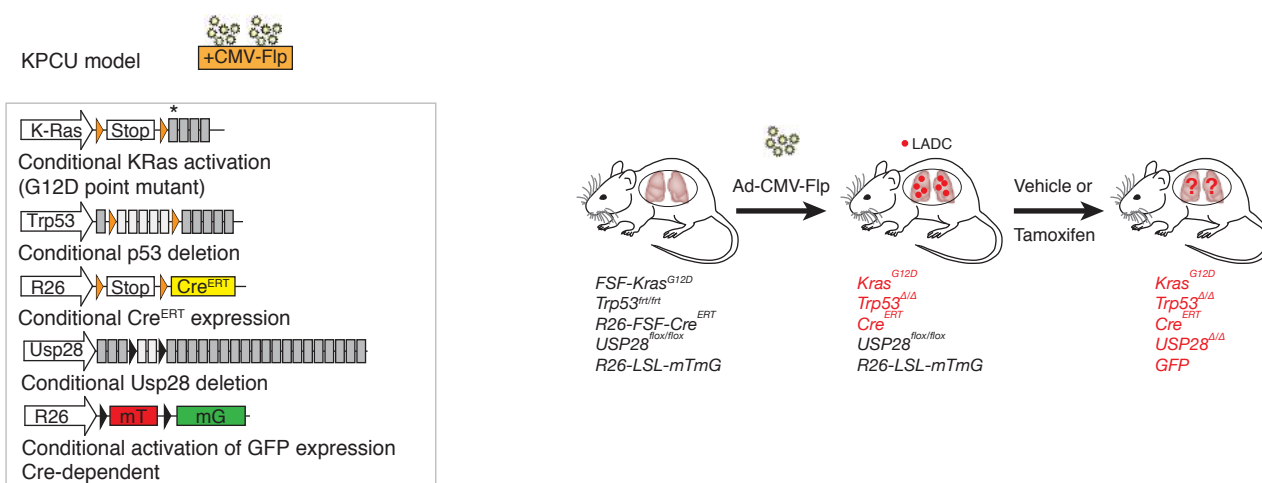
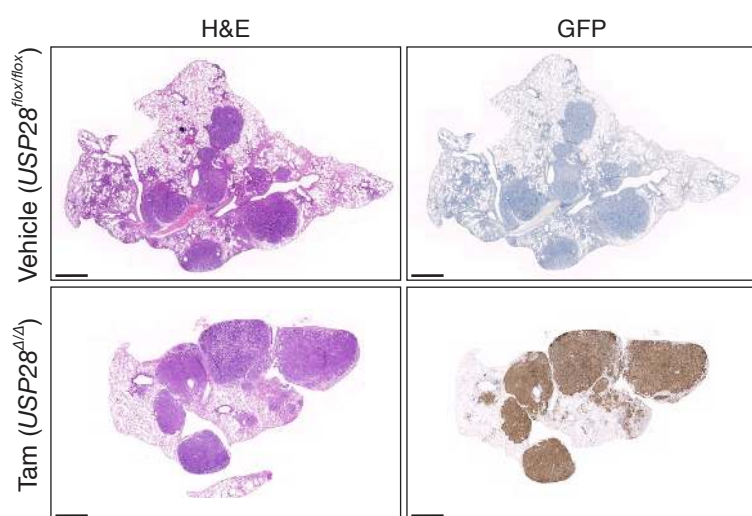


**Figure 2**

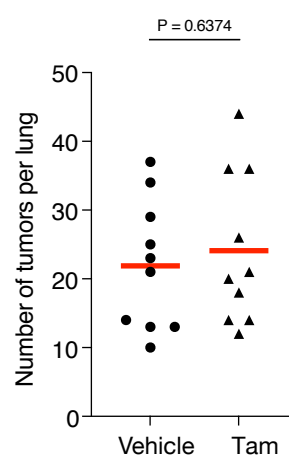
**A**



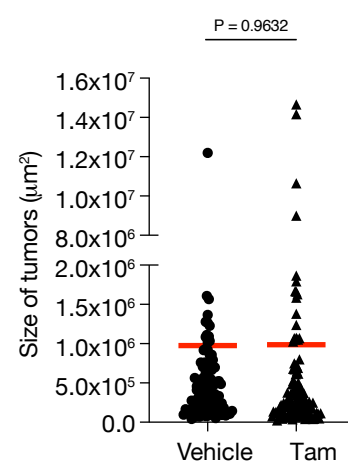
**B**



**C**



**D**



**E**

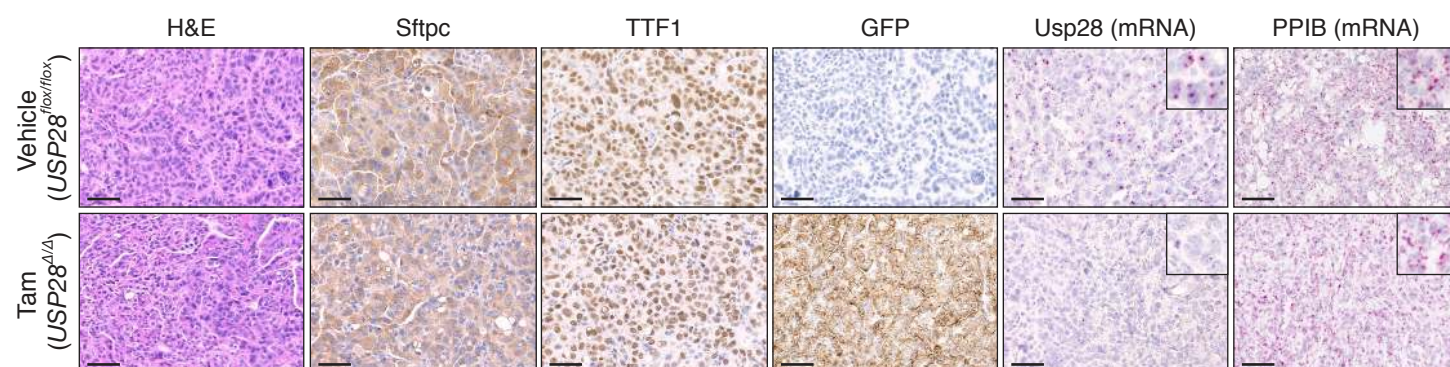
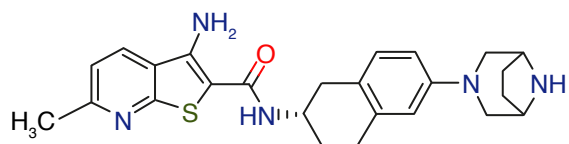


**Figure 3**

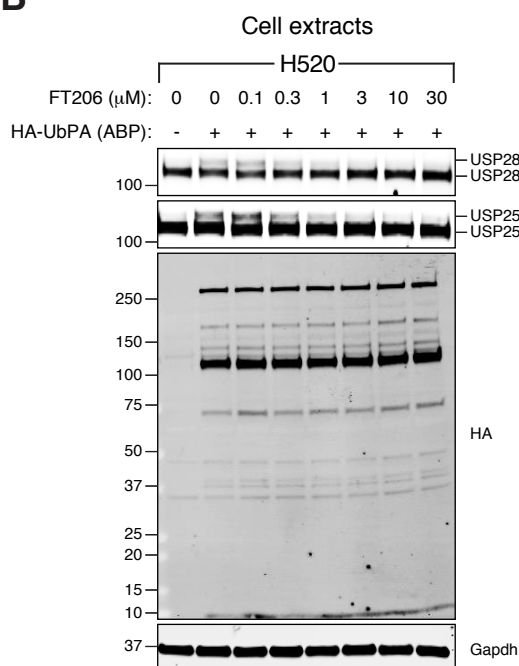
**A**



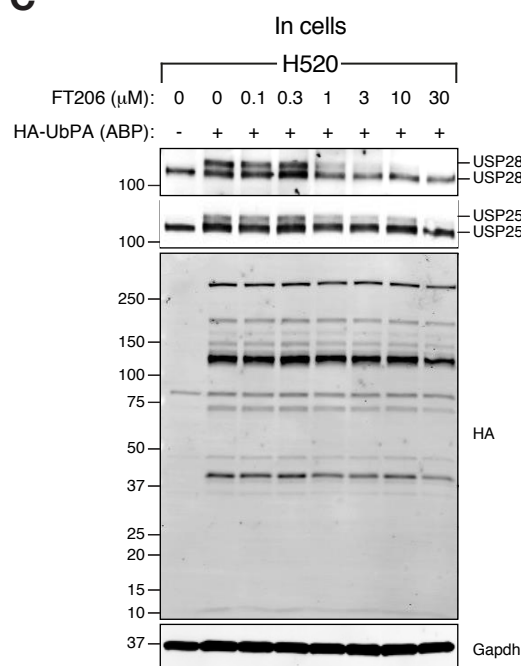
FT206

N-((2S)-6-(3,8-diazabicyclo[3.2.1]octan-3-yl)-1,2,3,4-tetrahydronaphthalen-2-yl)-3-amino-6-methylthieno [2,3-b] pyridine-2-carboxamide

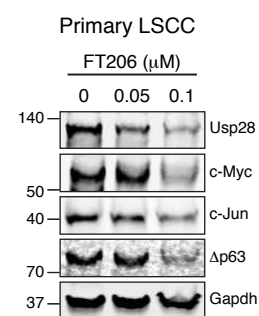
**B**



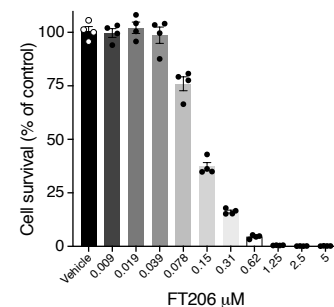
**C**



**E**



**F**



**D**

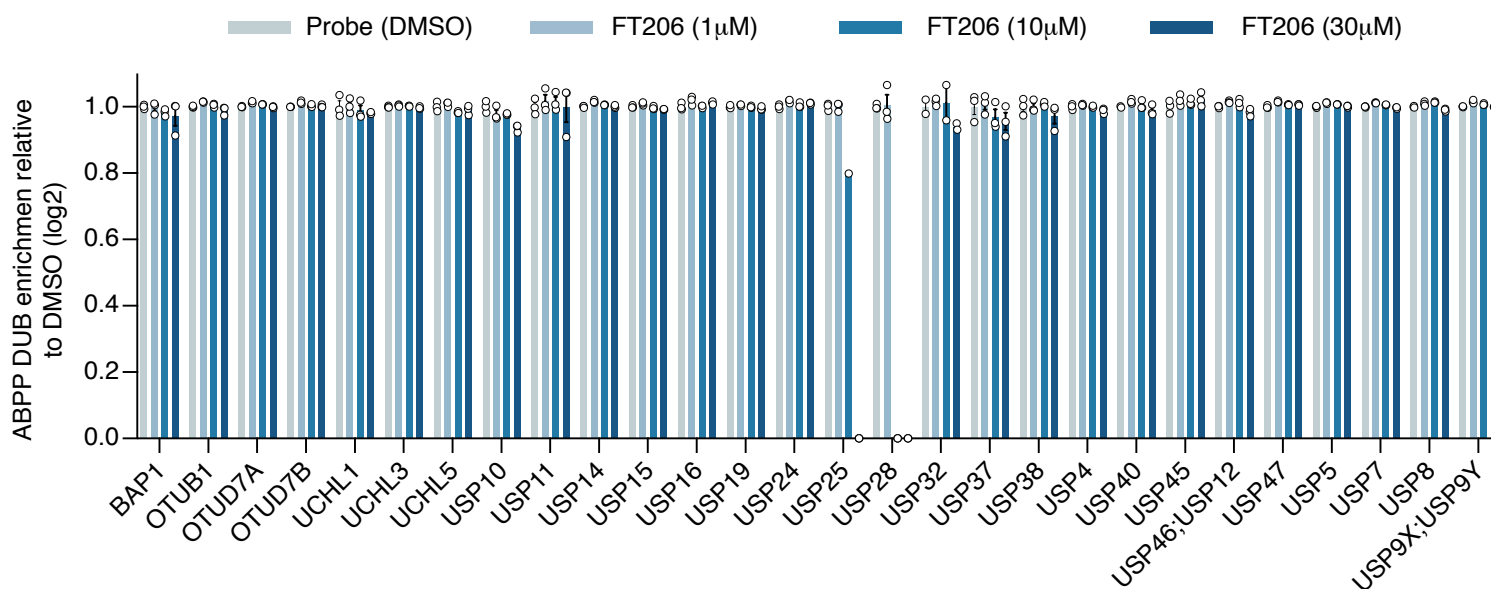
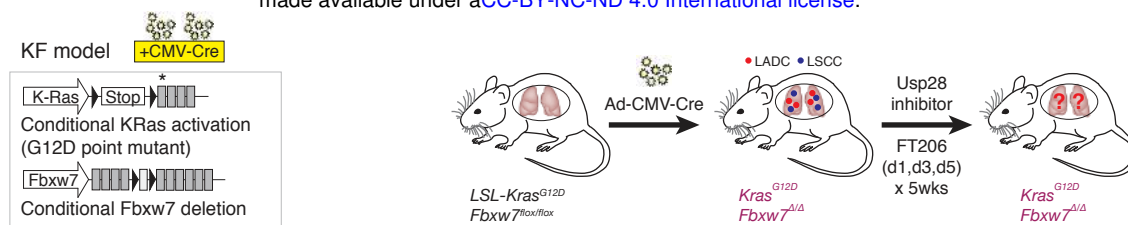
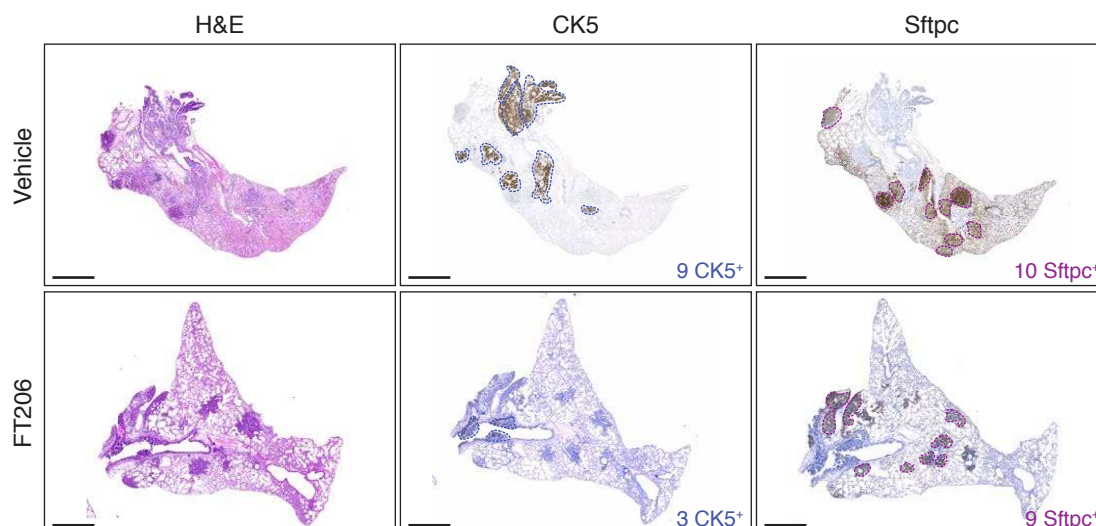


**Figure 4**

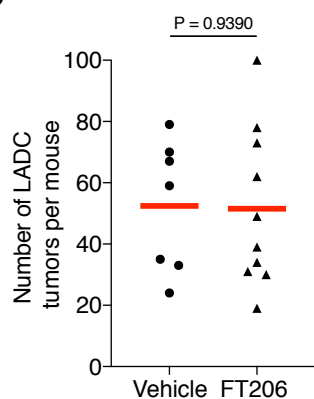
**A**



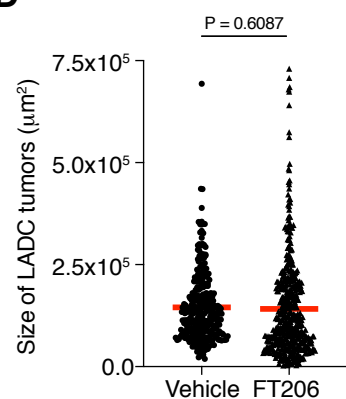
**B**



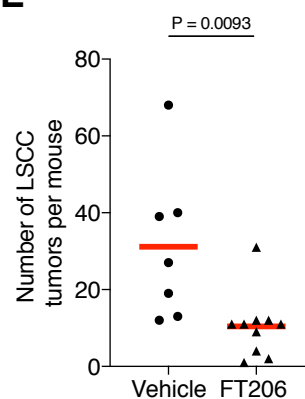
**C**



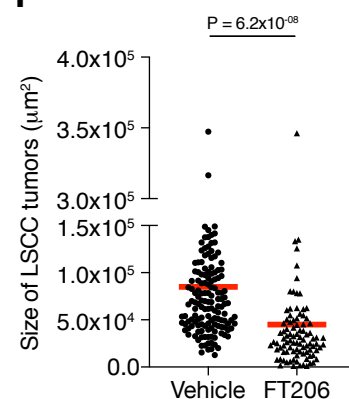
**D**



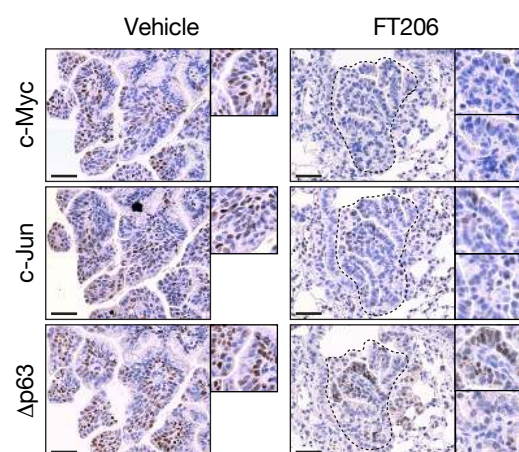
**E**



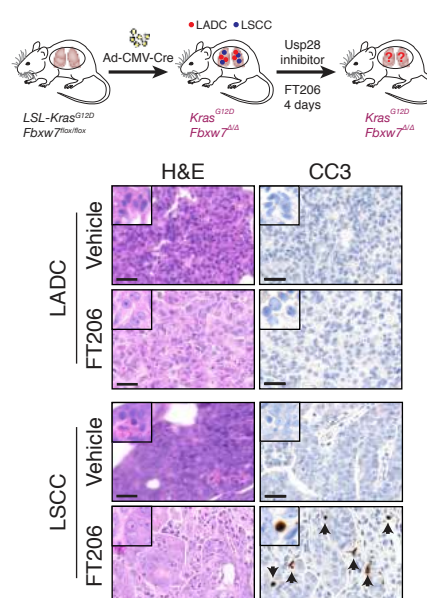
**F**



**G**



**H**



**I**

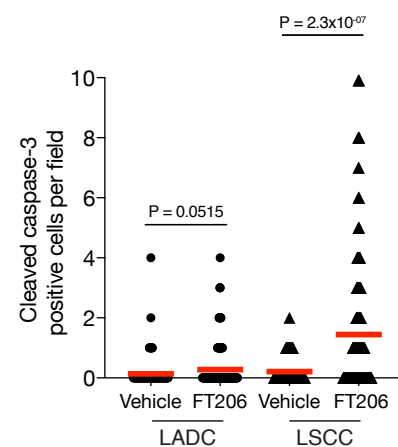


**Figure 5**

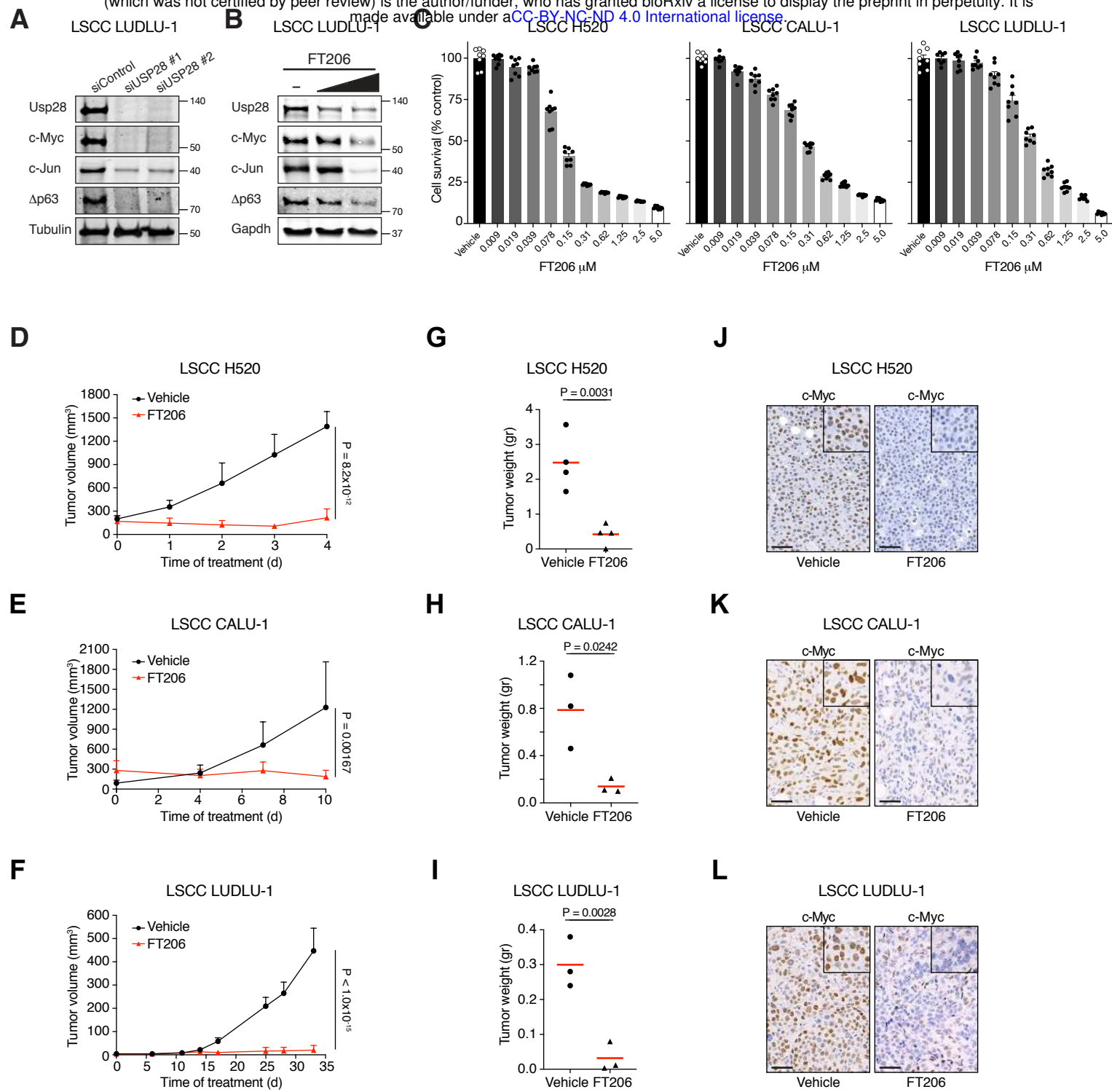
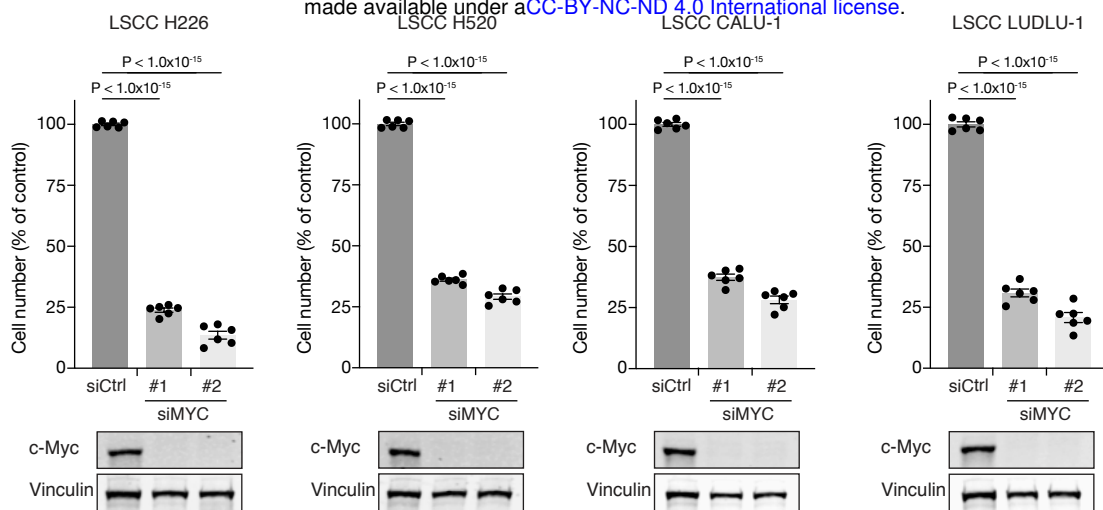
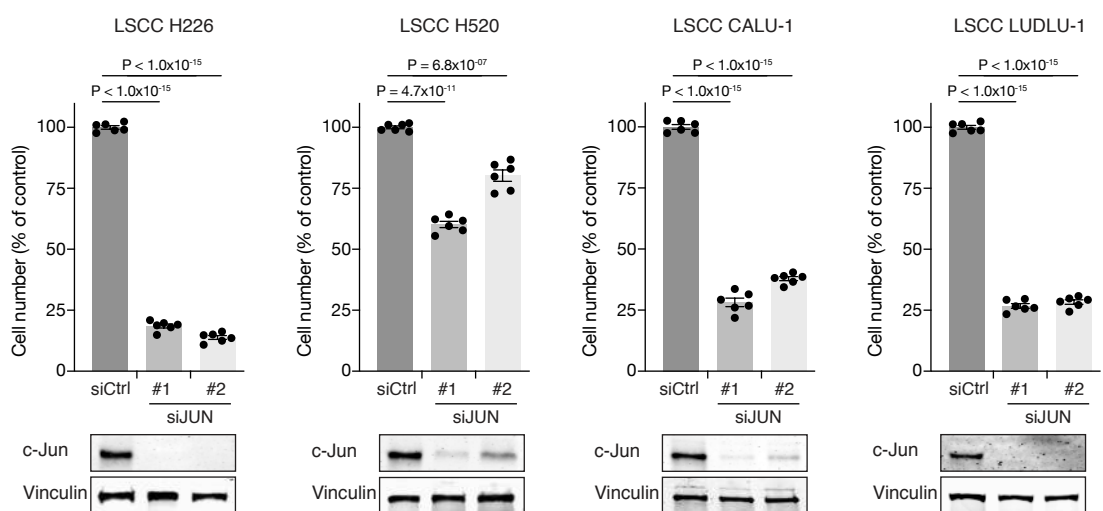


**Figure 6**

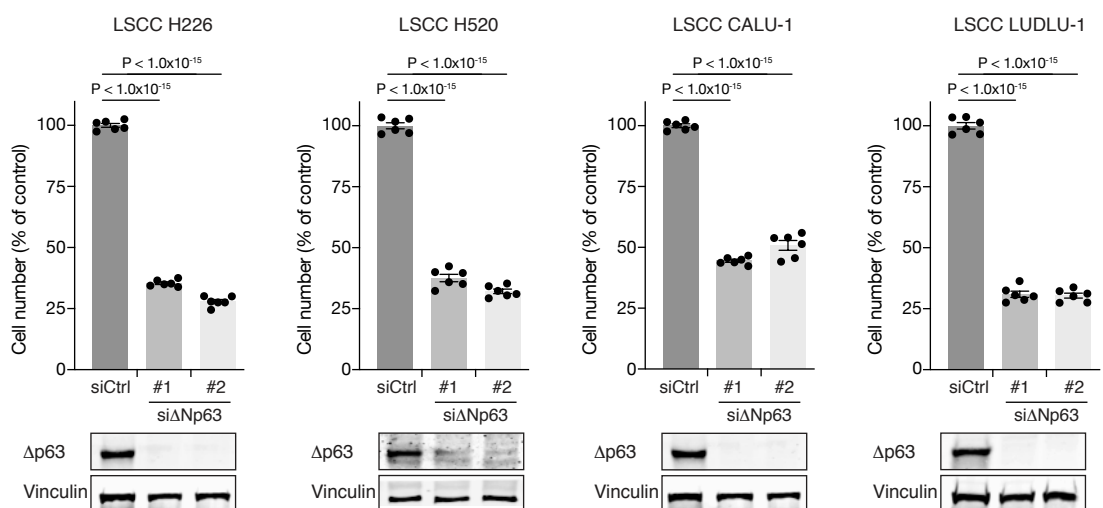
**A**



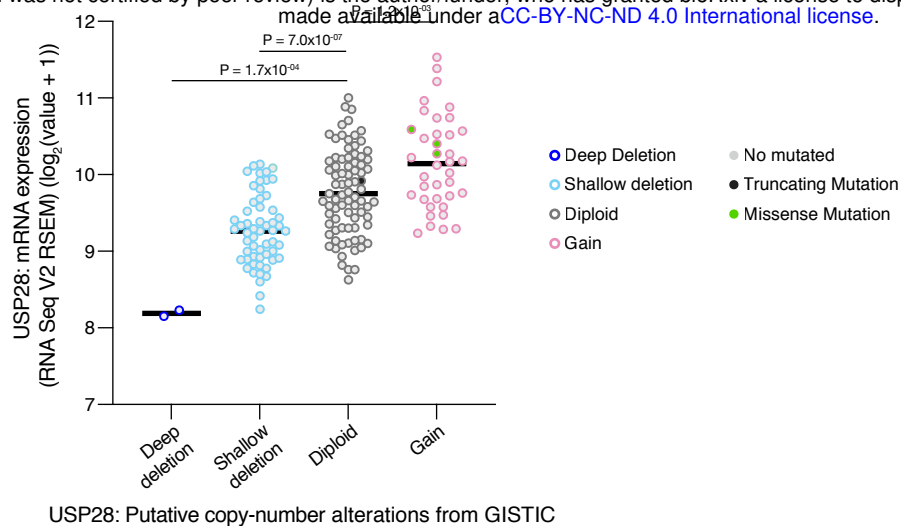
**B**



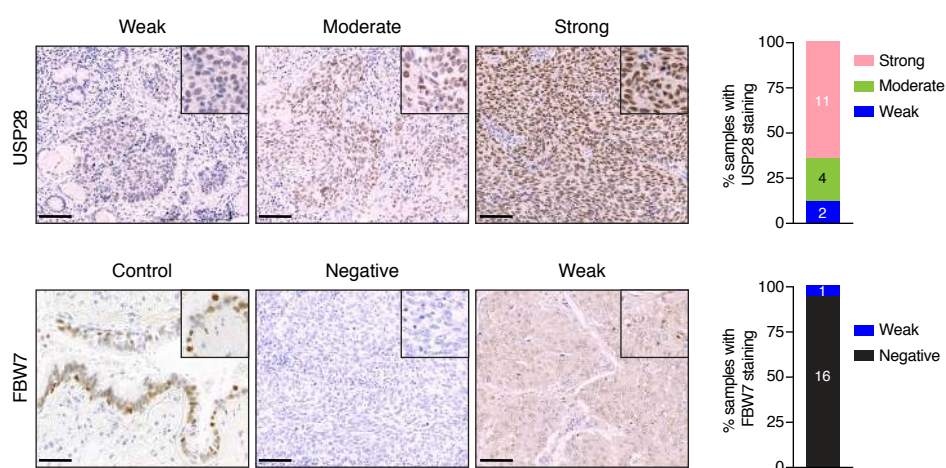
**C**



**A**



**B**



**A**

**Targeting intron 4**

oligo donor ...tgtagctagaattgccatgcctagccttttacaacgatggGAAGTTCCTATTCTCTAGAAAGTATAGGAACCTTCgatgggatccaagcccttatcttcattacacatga...  
 -60bp homology ← → -60bp homology

ccactgaatcgagagcttaccattcagctagagtgccagctgtccagtgagcagtgactgtagctagaattgccatgcctagccttttacaacgatgggatccaagcccttatcttcattacac  
 gRNA-Int4B

ggtgacttagctctcgaatgggtaagtcgatctcaccgtgcacaggtcactcgtcactgacatcgatcttaaacggtacggatcggaataatgttctaccccttaggttcgggaatagaagtagtaatgtg  
 gRNA-Int4A

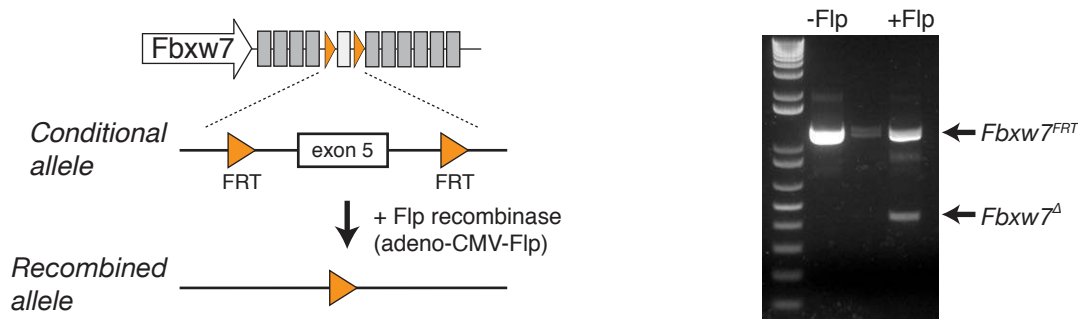
**Targeting intron 5**

oligo donor ...gccgtgtgaccaggtagagagcaactgacgagtgaggccatggGAAGTTCCTATTCTCTAGAAAGTATAGGAACCTTCcggaggagggaagactccagggtaggatc...  
 -60bp homology ← → -60bp homology

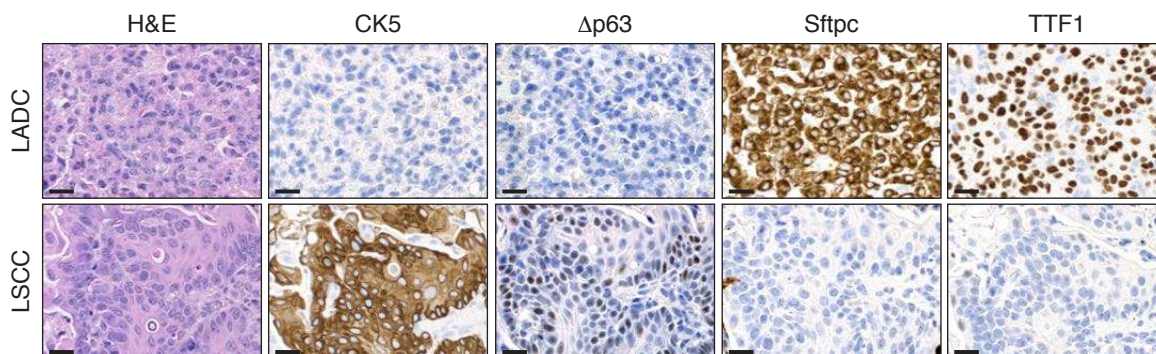
tggtaatgctctgttctatagatcagccoccttggcagccgtgtgaccaggtagagagcaactgacgagtgaggccatggaggagggaagactccagggtaggatcctcaggtgcttcttgctgagcctggt  
 gRNA-Int5B

accattacgagacaagatatctagtcggggaaccgtcggcacactggtccatctctcgtgactgctcactccgcctcctcctctctgaggtcccatcctagagtcacagaagaacgactcggacca  
 gRNA-Int5A

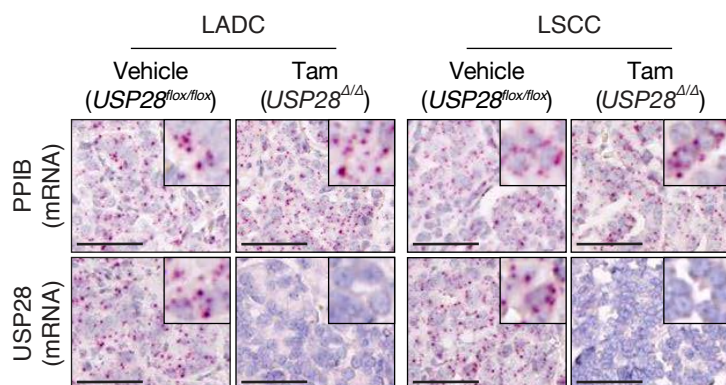
**B**



**C**



**D**



**E**

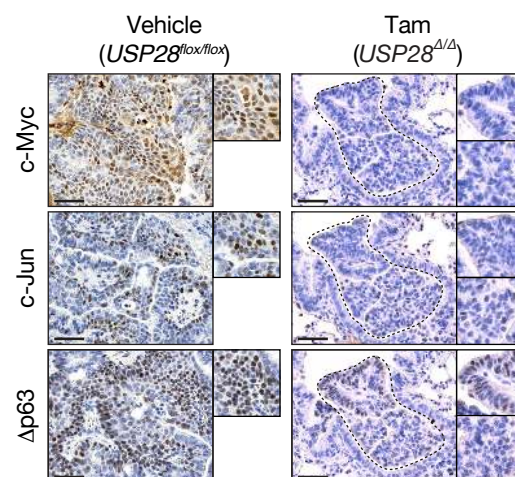
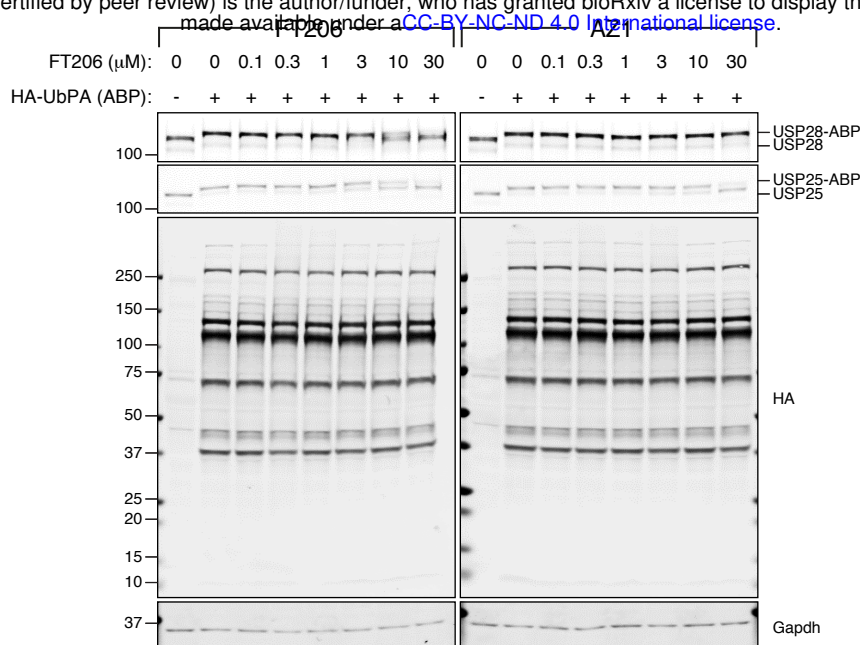


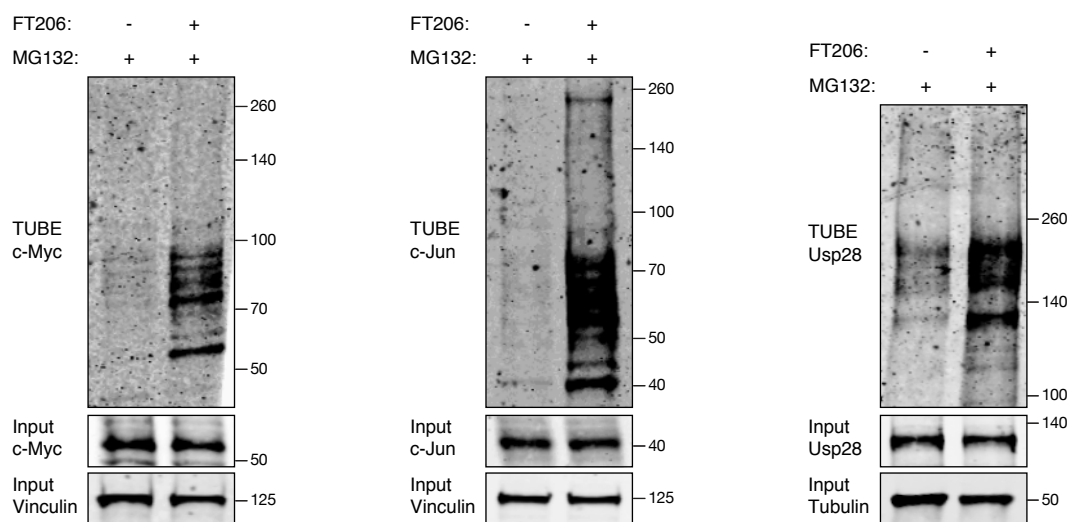
**Figure S3**



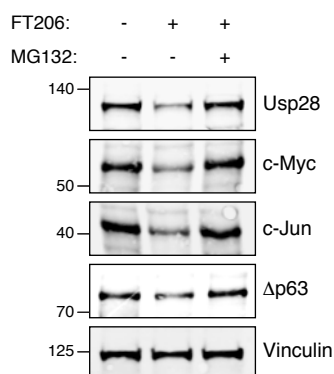
**A**



**B**



**C**



**D**

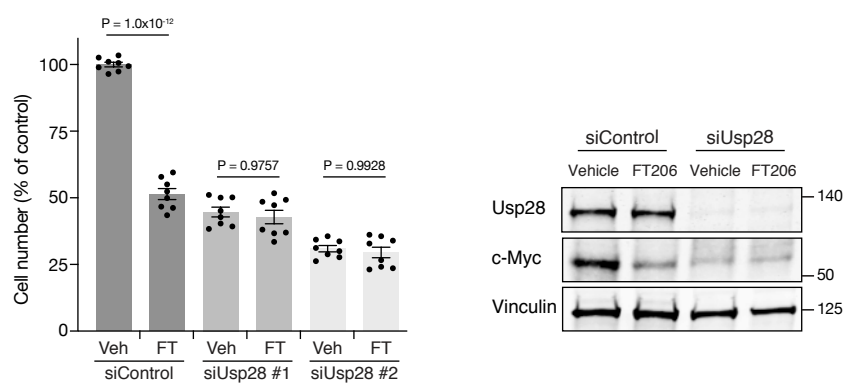
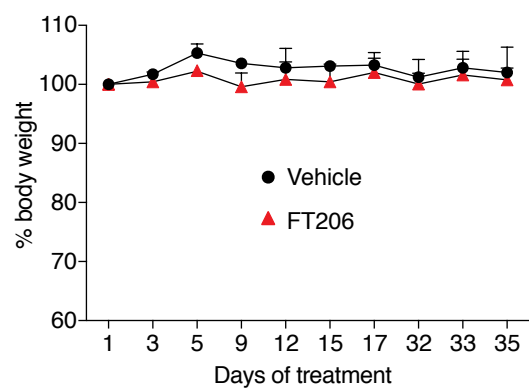


**Figure S4**

**A**



**B**

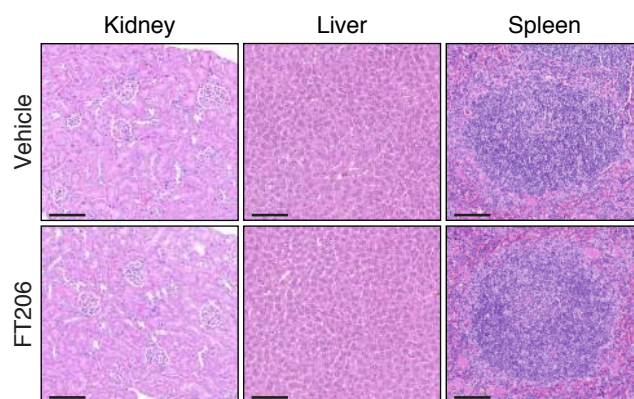
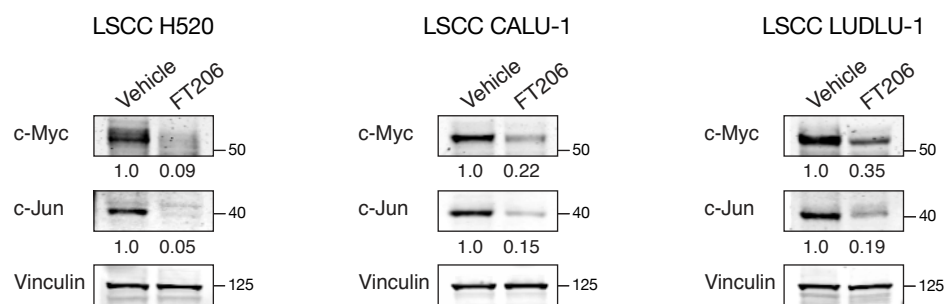
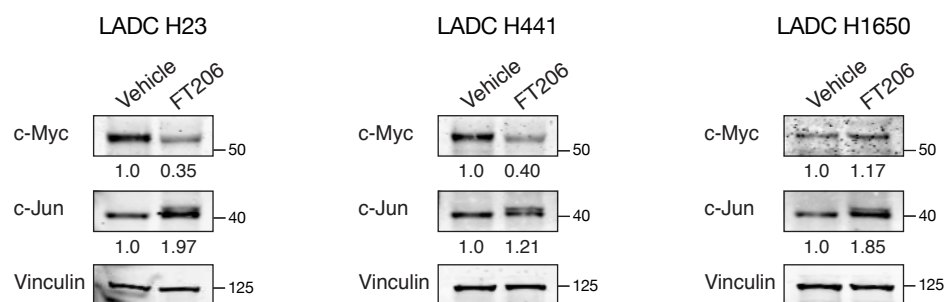


**Figure S5**

**A**



**B**



**C**

Cell line	IC50 ( $\mu$ M)
LSCC H520	0.1056
LSCC CALU-1	0.2221
LSCC LUDLU-1	0.3053
LADC H23	0.3062
LADC H441	1.25
LADC H1650	0.3920

**Figure S6**